# Elevated Ubiquitin Phosphorylation by PINK1 Contributes to Proteasomal Impairment and Promotes Neurodegeneration

Cong Chen[1,#], Tong-Yao Gao[1,#], Hua-Wei Yi[4], Yi Zhang[3], Tong Wang[1], Zhi-Lin Lou[1], Tao-Feng Wei[1], Yun-Bi Lu[1], Ting-Ting Li[3], Chun Tang[2,*], Wei-Ping Zhang[1,5,*]

[1] Department of Pharmacology, Zhejiang University School of Medicine, Hangzhou 310058, China

[2] Beijing National Laboratory for Molecular Sciences, College of Chemistry and Molecular Engineering, Center for Quantitate Biology, Center for Life Science, Academy for Advanced Interdisciplinary Studies, Peking University, Beijing 100871, China

[3] Department of Biomedical Informatics, School of Basic Medical Sciences, Peking University Health Science Center, Beijing 100191, China

[4] The First People's Hospital of Jingzhou, First Affiliated Hospital of Yangtze University, Jingzhou 121001, China

[5] Zhejiang Key Laboratory of Precision psychiatry, Hangzhou, 10003, China

[#] Equally contributed

*Corresponding authors

Chun Tang, Tang_Chun@pku.edu.cn, 292 Chengfu Road, Beijing 100871, China, 011-86-010-62751710

Wei-Ping Zhang, weiping601@zju.edu.cn, 866 Yuhangtang Rd, Hangzhou 310058, China, 011-86-0571-88208223

**Abstract**

Ubiquitin (Ub), a central regulator of protein turnover, can be phosphorylated by PINK1 (PTEN-induced putative kinase 1) to generate S65-phosphorylated ubiquitin (pUb). Elevated pUb levels have been observed in aged human brains and in Parkinson's disease, but the mechanistic link between pUb elevation and neurodegeneration remains unclear. Here, we demonstrate that pUb elevation is a common feature under neurodegenerative conditions, including Alzheimer's disease, aging, and ischemic injury. We show that impaired proteasomal activity leads to the accumulation of sPINK1, the cytosolic form of PINK1 that is normally proteasome-degraded rapidly. This accumulation increases ubiquitin phosphorylation, which then inhibits ubiquitin-dependent proteasomal activity by interfering with both ubiquitin chain elongation and proteasome-substrate interactions. Specific expression of sPINK1 in mouse hippocampal neurons induced progressive pUb accumulation, accompanied by protein aggregation, proteostasis disruption, neuronal injury, neuroinflammation, and cognitive decline. Conversely, *pink1* knockout mitigated protein aggregation in both mouse brains and HEK293 cells. Furthermore, the detrimental effects of sPINK1 could be counteracted by co-expressing Ub/S65A phospho-null mutant but exacerbated by over-expressing Ub/S65E phospho-mimic mutant. Together, these findings reveal that pUb elevation, triggered by reduced proteasomal activity, inhibits proteasomal activity and forms a feedforward loop that drives progressive neurodegeneration.

46 ## Introduction

47 Neurodegeneration, a hallmark of aging and neurodegenerative diseases, is
48 characterized by irreversible loss of neurons, ultimately leading to cognitive and motor
49 impairments (***Wilson et al.*, 2023**). A common feature of neurodegeneration is the
50 accumulation of ubiquitinated proteins, often resulting from the impairment of protein
51 degradation machineries, particularly the ubiquitin-proteasome system (UPS) (***Davidson and***
52 ***Pickering*, 2023; *Kinger et al.*, 2024; *McDade et al.*, 2024**). The UPS is essential for
53 maintaining cellular proteostasis, as it not only eliminates misfolded and toxic proteins but
54 also dynamically regulates neuronal structure and function through controlled protein
55 degradation (***Costa et al.*, 2019; *Krishna et al.*, 2022; *Soykan et al.*, 2021**). Substrate proteins
56 targeted for proteasomal degradation are typically conjugated with K48-linked polyubiquitin
57 chains, which interact non-covalently with ubiquitin receptors in the proteasome (***Komander***
58 ***and Rape*, 2012; *Pohl and Dikic*, 2019; *Swatek and Komander*, 2016**). However, UPS
59 activity can be compromised in neurodegeneration in multiple ways, including proteasome
60 modifications, reduced ATP level, direct inhibition by amyloid fibrils, and oxidative stress
61 (***Kinger et al.*, 2024; *McDade et al.*, 2024; *Tseng et al.*, 2008; *Wilson et al.*, 2023; *Wojcik***
62 ***and Di Napoli*, 2004**). While these factors have been extensively studied in order to preserve
63 proteasomal function, the dynamic changes of ubiquitin have been largely overlooked in the
64 context of neurodegeneration.

65 Ubiquitin itself undergoes post-translational modifications that can alter its structure
66 and function (***Herhaus and Dikic*, 2015**). One such modification is phosphorylation at
67 residue S65, installed by the kinase PINK1 (PTEN-induced putative kinase 1) (***Koyano et al.*,**
68 **2014**). PINK1 can exist in two forms: the full-length PINK1 localized to the mitochondrial
69 membrane (***Okatsu et al.*, 2015; *Okatsu et al.*, 2013**), and sPINK1, a cytosolic fragment

70 cleaved from full-length PINK1 (***Takatori et al.*, 2008; *Yamano and Youle*, 2013**). Full-
71 length PINK1 is activated in response to mitochondrial damages, subsequently
72 phosphorylating ubiquitin and Parkin to initiate mitophagy—a neuroprotective process for
73 the selective removal of damaged mitochondria (***Koyano et al.*, 2014; *Lazarou et al.*, 2015;**
74 ***Okatsu et al.*, 2015; *Wilson et al.*, 2023**). However, severe and persistent mitochondrial stress
75 can also lead to mitophagy failure and sustained elevations of S65-phosphorylated ubiquitin
76 (pUb) levels (***Chin et al.*, 2023; *Pollock et al.*, 2024**). Given the prevalence of mitochondrial
77 dysfunction under neurodegenerative conditions (***Wilson et al.*, 2023**), pUb accumulation
78 may result from the activation of full-length PINK1 but without effective mitophagy.

79 Alternatively, elevated pUb levels may arise from inhibited proteasomal degradation.
80 The cytosolic sPINK1, processed from the full-length PINK1 by mitochondrial proteases, is
81 normally rapidly degraded by the proteasome via the N-end rule pathway (***Takatori et al.*,**
82 **2008; *Yamano and Youle*, 2013**). As the UPS function is often compromised in
83 neurodegeneration (***Wilson et al.*, 2023**), sPINK1 may accumulate and phosphorylate
84 ubiquitin, contributing to the increased pUb levels.

85 Elevated levels of pUb have been observed in aged human brain and in Parkinson's
86 disease (***Fiesel et al.*, 2015; *Hou et al.*, 2018; *Shiba-Fukushima et al.*, 2017**). While pUb
87 elevation has been proposed as a potential biomarker of neurodegenerative diseases (***Fiesel et***
88 ***al.*, 2015; *Hou et al.*, 2018**), its functional role remains poorly understood. *In vitro* studies
89 have suggested that phosphorylation alters ubiquitin's structural dynamics and may affect its
90 function (***Dong et al.*, 2017; *Tang and Zhang*, 2020; *Wauer et al.*, 2015a**). Moreover,
91 PINK1 phosphorylation has been shown to inhibit ubiquitin chain elongation (***Wauer et al.*,**
92 **2015b**), and the phosphomimic mutant Ub/S65E has been show to inhibit protein turnover

93 and reduce cell viability under stress conditions in yeast (***Swaney et al.*, 2015**). As such,
94 elevated pUb levels may actively contribute to the progression of neurodegenerative diseases.

95 In the current study, we demonstrate that pUb levels are elevated in various
96 neurodegenerative conditions, including Alzheimer's disease (AD), aging, and ischemic
97 injury. Furthermore, we reveal that elevated pUb levels inhibit proteasomal activity, leading
98 to protein aggregation and neuronal damages. Upon investigating the underlying mechanism
99 at molecular, cellular and animal levels, we have uncovered a general pathogenic pathway
100 involving pUb that operates across a wide spectrum of neurodegenerative disorders.

## 101 Results

### 102 Elevated pUb levels are a pervasive feature of neurodegeneration

103 Elevated pUb levels have been observed in the brains of individuals with Parkinson's
104 disease (PD) (***Fiesel et al.*, 2015; *Hou et al.*, 2018; *Shiba-Fukushima et al.*, 2017**). In the
105 current study, we extend this observation to Alzheimer's disease (AD), the most prevalent
106 neurodegenerative dementia. We found a marked elevation of both PINK1 and pUb in brain
107 samples from AD patients in the cingulate gyrus brain regions with Aβ plaques, when
108 compared to age- and sex-matched controls (***Figure 1A, B; Figure 1—table supplementary***
109 ***1***). This finding was corroborated in the APP/PS1 mouse model of AD, where increased
110 PINK1 and pUb levels could be detected in neocortex of mouse brains with Aβ compared to
111 wildtype mice (***Figure 1C, D***). On the other hand, PINK1 and pUb levels in neocortex of
112 wildtype and *pink1*-knockout mice (*pink1-/-*) differ little (***Figure 1C, D***), which can be
113 attributed to the low expression of PINK1 in normal mouse brains under physiological
114 conditions.

115 Beyond the specific neurodegenerative diseases, pUb elevation also appears to be
116 associated with aging process (***Fiesel et al.*, 2015; *Hou et al.*, 2018**), a special pathological
117 condition that is often accompanied by gradual neurodegeneration. The difference of PINK1
118 expression between young and aged mouse cortex was not distinguishable due to the low
119 expression level and probably also due to specificity of PINK1 antibody used. However, we
120 observed a significant increase in neuronal pUb levels in aged wildtype mouse compared to
121 young mouse in neocortex of the brains (***Figure 1E, F***). As a control, pUb levels in *pink1*-/-
122 mice remained unchanged with age and were notably lower than those in aged wild-type
123 mice (***Figure 1E, F***). As such, although the pUb antibody may not be highly specific, the
124 observed increase in immunofluorescence and protein band intensities, when comparing
125 across different *pink1* genetic background, can only be attributed to elevated pUb levels
126 during aging.

127 We further showed that acute neurodegenerative conditions, such as cerebral ischemia,
128 are also associated with elevated pUb levels. Using mouse middle cerebral artery occlusion
129 (MCAO) model, we observed a marked increase in both PINK1 and pUb levels in the
130 penumbra of mouse brains compared to the contralateral cortex (***Figure 1G, figure 1—figure***
131 ***supplementary 1***). To further explore the relationship between pUb and ischemic stress, we
132 subjected HEK293 cells to oxygen-glucose deprivation (OGD), a cellular model mimicking
133 ischemic conditions. OGD followed by reperfusion caused a time-dependent increase in
134 PINK1, sPINK1, and pUb levels (***Figure 1H***). Additionally, we observed an increase of
135 protein aggregation, as evidenced by the accumulation of ubiquitin in the insoluble protein
136 fraction (***Figure 1I***).

137 Taken together, these findings demonstrate that elevated pUb levels are a common
138 feature across a wide spectrum of neurodegenerative conditions, both chronic and acute.

While our observation support the notion of pUb as a biomarker, the diverse functions of ubiquitin suggest that elevated pUb levels may actively contribute to the pathogenesis of neurodegeneration.

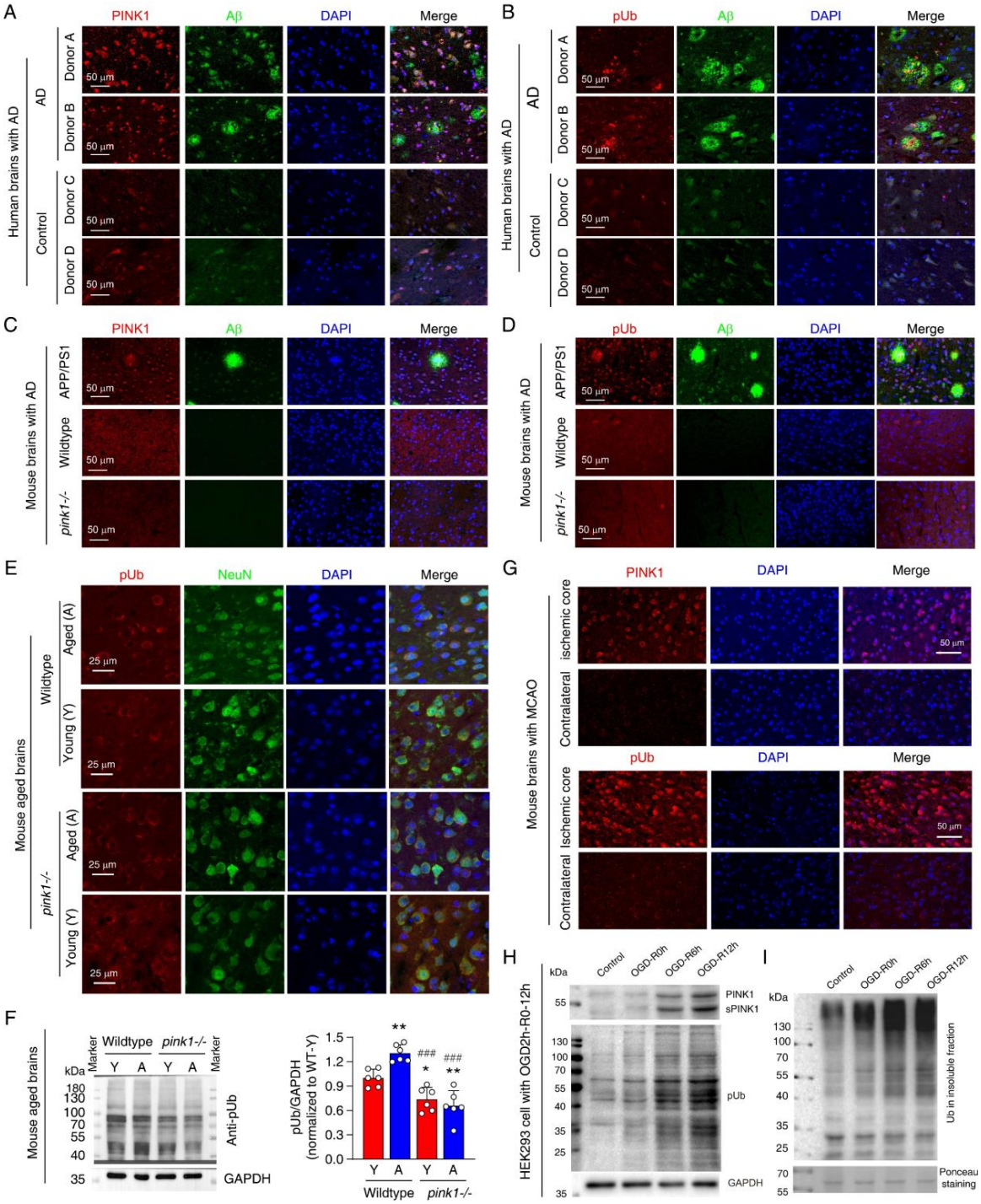


**Figure 1. Elevated pUb levels are widespread across neurodegenerative conditions.**

144 **(A, B)** Double immunofluorescence staining showing the distribution of PINK1 and Aβ (A), and pUb
145 and Aβ (B), within the cingulate gyrus brain region of AD patients compared to similar brain regions
146 from age-matched controls. Detailed donor information is provided in ***Supplementary Table 1***.

147 **(C, D)** Double immunofluorescence staining of PINK1 and Aβ (C), and pUb and Aβ (D) in the brains
148 of wildtype, *pink1-/-*, and APP/PS1 transgenic mice. The images were taken for the neocortex of
149 APP/PS1, wildtype, and *pink1-/-* mice.

150 **(E)** Double immunofluorescence staining for pUb and the neuronal marker NeuN in the neocortex of
151 young and aged brains of both wildtype and *pink1-/-* mice. The images were taken for the layer III-IV
152 of neocortex.

153 **(F)** Western blot analysis of pUb levels in the cortex of young (Y) and aged (A) wildtype and *pink1-/-*
154 mouse brains, quantitatively comparing protein levels across ages and genotypes. $^{*}P<0.05$, $^{**}P<0.01$
155 for comparisons with young wildtype mice; $^{\#\#\#}P<0.001$ for comparisons with aged wildtype mice,
156 one-way ANOVA.

157 **(G)** Immunofluorescence staining for PINK1 and pUb in the contralateral and penumbra of mouse
158 brains subjected to MCAO for 2 hours, followed by 24 hours of reperfusion. Locations of the
159 analyzed brain regions are shown in ***Figure 1-supplemary figure 1***.

160 **(H)** Western blot analysis of PINK1 and pUb levels in HEK293 cells subjected to OGD for 2 hours,
161 followed by reperfusion at 0, 6, and 12 hours.

162 **(I)** Western blot analysis of ubiquitin in the insoluble fraction of HEK293 cells post 2-hour OGD and
163 subsequent 0, 6, 12 hours of reperfusion.

164

165 **Ubiquitin phosphorylation by sPINK1 impairs proteasomal function in HEK293 cells**

166 Elevated pUb levels can result from either elevated level of full-length PINK1 or
167 sPINK1. PINK1 increase can occur upon mitochondrial injuries with the treatment of CCCP
168 and O/A, and sPINK1 increase can occur upon proteasomal inhibition with the treatment of
169 MG132 (***Figure 2A***). The treatment of MG132 caused a concentration- and time-dependent
170 increase in sPINK1 and pUb levels in wildtype HEK293 cells, with sPINK1 levels plateaued
171 at 6 hours (***Figures 2B-E***). In contrast, PINK1 and pUb levels remained low in *pink1-*
172 knockout HEK293 cells upon the treatment of MG132 (***Figures 2B-E***).

173 While PINK1 activation typically involves its dimerization at mitochondrial outer
174 membrane (***Gan et al.*, 2022; *Okatsu et al.*, 2013**), we investigated whether cytoplasmic
175 sPINK1 retains activity of phosphorylating ubiquitin. We transiently transfected HEK293

176 cells with several PINK1 constructs: full-length PINK1, a cytoplasmic variant of sPINK1 that
177 is more resistant to UPS degradation (sPINK1*, PINK1/F101M/L102-L581, differing from
178 the native sequence by the N-terminal Met instead of Phe), a kinase-dead version of this
179 stable variant (sPINK1*-KD, with K219A/D362A/D384A mutations introduced) (***Beilina et***
180 ***al.*, 2005**), and $Ub^{GG}$-sPINK1, a short-lived version of native-sequence sPINK1 with a
181 ubiquitin appended at the N-terminus (***Yamano and Youle*, 2013**). Western blot analysis
182 confirmed the expression of PINK1, sPINK1* and sPINK1*-KD following transfection,
183 while $Ub^{GG}$-sPINK1 was undetectable due to its rapid degradation (***Figure 2F***). The analysis
184 also showed elevated pUb levels upon the transfection of full-length PINK1 and sPINK1*,
185 with the latter more pronounced. In contrast, transfection with sPINK1*-KD or $Ub^{GG}$-
186 sPINK1 had little effect on pUb levels (***Figure 2F***).

187 Furthermore, immunofluorescence staining revealed a diffuse cytoplasmic ubiquitin
188 distribution in non-transfected or eGFP-transfected control cells. In contrast, ubiquitin-
189 positive puncta were observed following MG132 treatment or upon the transfection of
190 sPINK1* (***Figure 2G***). Weak ubiquitin-positive puncta were also visible in $Ub^{GG}$-sPINK1-
191 transfected cells (***Figure 3G***, $5^{th}$ row, indicated by arrows), likely due to a slight elevation in
192 sPINK1 level. Furthermore, Western blot analysis showed that MG132 treatment and
193 sPINK1* transfection (***Figure 2H***), but not sPINK1*-KD or $Ub^{GG}$-sPINK1 transfection,
194 increased ubiquitin levels in the insoluble protein fraction. These findings suggest a positive
195 correlation between PINK1 and pUb levels and the aggregation of ubiquitinated proteins,
196 which likely results from an impairment of proteasomal activity, akin to the effect of MG132.

197 To confirm the inhibitory effect of pUb on proteasomal activity, we transfected cells
198 with Ub-R-GFP, a model substrate for the proteasome (***Dantuma et al.*, 2000; *Samant et al.*,**
199 **2018**). GFP was rapidly degraded by functional proteasomes but accumulated upon the

200 administration of MG132. Transfection with sPINK1* also caused GFP accumulation, but the
201 transfection of sPINK1*-KD did not (***Figure 2I***). Thus, sPINK1* transfection leads to
202 increased pUb levels and impairs proteasomal degradation.

203 Elevated pUb levels may also lead to protein aggregation by inhibiting autophagic
204 degradation. To assess the involvement of this pathway, we treated HEK293 cells with
205 puromycin to increase ubiquitinated protein level, which can be degraded through both
206 autophagic and UPS pathways (***Figure 2I***). The ubiquitin signal was significantly lower in
207 the sPINK1*-transfected cells compared to neighboring non-transfected cells (***Figure 2J***),
208 indicating that sPINK1* promotes the degradation of ubiquitinated proteins. However, when
209 we blocked autophagic degradation using BALA (***Mauvezin and Neufeld*, 2015**), ubiquitin
210 signal was higher in the sPINK1*-transfected cells compared to non-transfected cells (***Figure***
211 ***2J***), indicating sPINK1* inhibits the degradation of ubiquitinated protein. Taken together, the
212 findings demonstrate that while sPINK1* can enhance autophagic degradation of
213 ubiquitinated proteins, potentially through p62 phosphorylation as previously reported (***Gao***
214 ***et al.*, 2016**), elevated PINK1 and pUb levels cause an inhibition of proteasomal degradation.

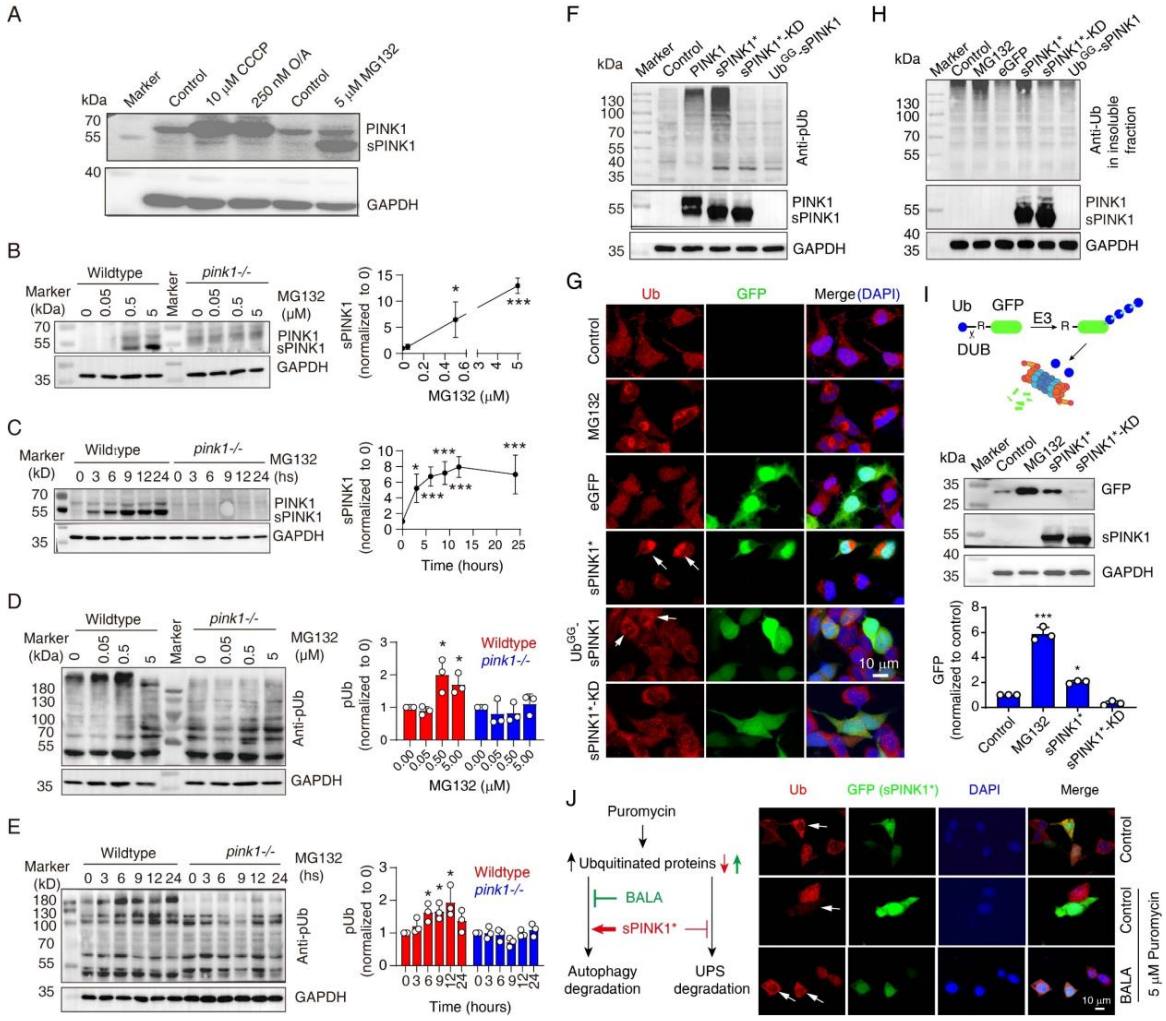


**Figure 2. Ubiquitin phosphorylation by sPINK1 affects proteasomal activity in HEK293 cells.**

**(A)** Representative Western blot showing the levels of PINK1 following the administration of CCCP, O/A, or MG132. The CCCP was treated for 12 hours, O/A was treated for 2 hours, and the MG132 was treated for 8 hours.

**(B)** Western blot analysis showing the concentration-dependent effect of MG132 (0-5 μM) over an 8-hour period on PINK1 level. $N$=3; *$P$ < 0.05, ***$P$ < 0.001, compared to 0 μM MG132, one-way ANOVA.

**(C)** Western blot analysis showing the time-dependent effect of 5 μM MG132 on PINK1 levels in 0-24 hours. $N$=4; *$P$ < 0.05, ***$P$ < 0.001, compared to 0 hours, one-way ANOVA.

**(D)** Western blot analysis of pUb levels under a concentration gradient of MG132 (0-5 μM) for 8 hours. $N$=3; *$P$ < 0.05, compared to 0 μM MG132, one-way ANOVA.

**(E)** Western blot analysis of pUb levels over a time course of 0-24 hours with 5 μM MG132 treatment. $N$=3; *$P$ < 0.05, compared to 0 hours, one-way ANOVA.

**(F)** Representative Western blot image showing the levels of pUb and PINK1 at 24 hours post-transfection with different PINK1 constructs: sPINK1* (PINK1/F101M/L102-L581), sPINK1*-KD

231 (kinase-dead sPINK1* with additional K219A/D362A/D384A mutations), and $Ub^{GG}$-sPINK1 (a
232 short-lived version of native sPINK1 with an appended N-terminal Ub).

233 **(G)** Representative immunofluorescence images of ubiquitin staining in cells treated with 5μM
234 MG132 for 8 hours or transfected with different sPINK1 constructs, highlighting differences in
235 ubiquitin localization and aggregation. The white arrows indicate positively transfected cells.

236 **(H)** Representative Western blot image of ubiquitin in the insoluble protein fraction of cells. The cells
237 were collected at 8 hours after treatment with 5 μM MG132, or collected at 24 hours after transfection
238 with different sPINK1 constructs.

239 **(I)** Western blot analysis showing GFP degradation in HEK293 cells transfected with Ub-R-GFP.
240 Cells were harvested at 8 hours after 5 μM MG132 treatment, or 24 hours following sPINK1* or
241 sPINK1*-KD transfection. $N$=3; *$P$ < 0.05, ***$P$ < 0.001, compared to the control, one-way ANOVA.

242 **(J)** Immunofluorescence staining of ubiquitin illustrating how sPINK1 over-expression impacts on
243 proteasomal and autophagic degradation. Puromycin blocks protein synthesis at the translation
244 elongation stage, leading to the production of truncated proteins; BALA (bafilomycin A1, a v-ATPase
245 inhibitor) blocks the degradation of autophagic cargo by inhibiting autophagosome-lysosome fusion,
246 as illustrated in the left panel. Puromycin (5 μg/ml) was applied for 2 hours before harvesting with or
247 without the treatment of 0.1 μM BALA. The white arrows indicate positively transfected cells.

248

249 **pUb impairs proteasomal activity through both covalent and noncovalent mechanisms**

250 To elucidate how elevated pUb levels inhibit UPS activity, we first assessed ubiquitin
251 chain formation *in vitro*. While the unmodified ubiquitin efficiently formed di-, tri-, and
252 higher-order chains catalyzed by E1 and E2 enzymes, pUb predominantly formed di-Ub
253 chains (***Figure 3A***), consistent with the previous report (***Wauer et al.*, 2015b**). The
254 introduction of S65A (phospho-null) and S65E (phospho-mimetic) ubiquitin mutants further
255 confirmed the impact of phosphorylation—Ub/S65A mutation did not affect chain elongation,
256 producing a polyUb ladder similar to unmodified ubiquitin, while Ub/S65E mutation only
257 formed di-Ub (***Figure 3A***).

258 Furthermore, we examined ubiquitin chain formation in HEK293 cells by expressing
259 FLAG-Ub/48K, a ubiquitin mutant that can only form K48-linked ubiquitin chain. Upon
260 proteasomal inhibition with MG132, K48-linked chains were observed in wildtype and
261 *pink1-/-* cells, but were absent in cells over-expressing full-length PINK1 or sPINK1*

262 (***Figure 3B***), This further confirms the inhibitory effect of S65 phosphorylation on ubiquitin
263 chain elongation.

264 Since PINK1 can phosphorylate both ubiquitin monomers and polyUb chains (***Shiba-***
265 ***Fukushima et al.*, 2014**), we next investigated how polyUb phosphorylation impacts
266 proteasomal degradation. Using an *in vitro* degradation assay using purified proteasomes, we
267 found that the degradation of K48-linked pUb-chain-modified GFP (pK48-polyUb-GFP) was
268 slower compared to its unmodified counterpart (K48-polyUb-GFP) (***Figure 3C, figure***
269 ***3—figure supplementary 1, 2***). Additionally, we employed total internal reflection
270 fluorescence (TIRF) microscopy, following an established protocol (***Lu et al.*, 2015**), to
271 assess interactions between ubiquitinated substrate proteins and immobilized proteasomes.
272 The assay revealed fewer GFP puncta for pK48-polyUb-GFP compared to K48-polyUb-GFP
273 (***Figure 3D, E, figure 3—figure supplementary 3***). Furthermore, the GFP puncta for pK48-
274 polyUb-GFP dissociated more rapidly from the proteasomes, reflecting a shorter dwell time
275 of the proteasome-substrate complex (***Figure 3F-I, figure 3—figure supplementary 4***). Thus,
276 phosphorylation impairs the noncovalent interactions between polyUb chains conjugated to
277 substrate proteins and the ubiquitin receptors residing in the proteasome.

278 Together, these findings demonstrate that elevated pUb levels disrupt proteasomal
279 function through two distinct mechanisms: impairing covalent ubiquitin chain elongation and
280 substrate ubiquitination, as well as weakening non-covalent interactions between
281 ubiquitinated substrates and the proteasome. Both mechanisms collectively contribute to the
282 inhibition of ubiquitin-dependent proteasomal activity.

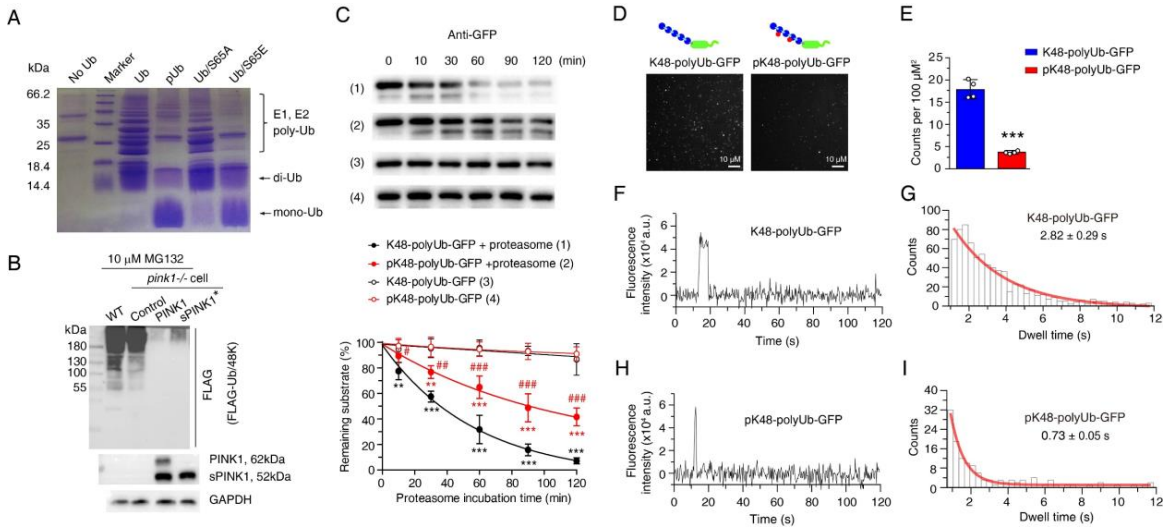


**Figure 3. Ubiquitin phosphorylation inhibits both ubiquitin chain elongation and ubiquitin proteasome interactions.**

**(A)** Coomassie blue staining showing ubiquitin chain formation/elongation using different ubiquitin variants as building blocks: wildtype ubiquitin, phosphorylated ubiquitin (pUb), phospho-null Ub/S65A, and phospho-mimic Ub/S65E.

**(B)** Western blot showing the formation of K48-linked ubiquitin chain in wildtype (WT) and *pink1-/-* HEK293 cells without or with PINK1 and sPINK1* transfection. Cells were transfected with FLAG-tagged Ub/48K to form K48-linked ubiquitin chain only, and 10 μM MG132 was applied at 12 hours post-transfection to prevent the degradation of ubiquitinated substrates.

**(C)** Western blot analysis of *in vitro* proteasomal degradation of GFP modified with K48-linked ubiquitin chains (K48-polyUb-GFP) and GFP modified with phosphorylated K48-linked ubiquitin chains (pK48-polyUb-GFP). $N$=3; $^{**}P<0.01$, $^{***}P<0.001$ compared to respective controls without added proteasome; $^{\#}P<0.05$, $^{\#\#}P<0.01$, $^{\#\#\#}P<0.001$ compared to K48-polyUb-GFP with proteasome, two-way ANOVA.

**(D)** Representative TIRF microscopy images showing single-molecule association of K48-polyUb-GFP (left) and pK48-polyUb-GFP (right) to the surface-immobilized proteasomes, visualized as bright puncta. Details of TIRF single-molecule visualization is shown in ***Figure 3—figure supplementary 3***.

**(E)** Quantitative analysis of puncta density from TIRF images comparing the number of puncta of K48-polyUb-GFP and pK48-polyUb-GFP associated with surface-immobilized proteasomes. $N$=4; $^{***}P<0.001$ compared to K48-polyUb-GFP, using a paired $t$-test.

**(F, H)** Representative fluorescence time traces of a single punctum for proteasomal bind K48-polyUb-GFP (F) and pK48-polyUb-GFP (H). More representative figures of single-molecule fluorescence are shown in in ***Figure 3—figure supplementary 4***.

**(G, I)** Analysis of GFP fluorescence dwell time for K48-polyUb-GFP (G) and pK48-polyUb-GFP (I) associated with the proteasome. Data were binned and modeled with a single exponential decay curve (red line).

312 ***pink1* knockout mitigates protein aggregation under neurodegenerative conditions**

313 Having established the causative link between elevated pUb levels and proteasomal
314 inhibition, we further explored the relationship with protein aggregation and whether *pink1*
315 knockout mitigates this process. We treated wildtype and *pink1-/-* HEK293 cells with MG132,
316 which increased insoluble ubiquitin levels in both cell types in a concentration- and time-
317 dependent manner (***Figure 4A, B***). However, insoluble ubiquitin levels accumulated
318 significantly slower in *pink1-/-* cells, though eventually reaching levels comparable to those
319 in wildtype cells (***Figure 4B***). This not only confirms that PINK1/pUb operates within the
320 same pathway as MG132—the proteasome—but also demonstrates that PINK1 deficiency
321 delays the accumulation of protein aggregates. MG132 treatment also elevated the levels
322 LC3-II, a marker of autophagy, in wildtype cells, indicating either autophagy activation or
323 reduced LC3 degradation in response to proteasomal inhibition (***Figure 4C, D***). However,
324 LC3-II levels did not increase in *pink1-/-* cells following MG132 treatment (***Figure 4C, D***).
325 This confirms the critical role of PINK1 in the activation of for autophagy (***Figure 2J***).

326 Furthermore, *pink1* knockout mitigated protein aggregation in animal models. In young
327 wildtype mouse brains, ubiquitin was evenly distributed in the neurons in neocortex, but
328 formed ubiquitin positive puncta in aged wildtype mouse brains (***Figure 4E***). Western blot
329 analysis revealed elevated levels of insoluble ubiquitin in the cortex of aged mice compared
330 to young mice (***Figure 4F***), further supporting age-related protein aggregation. In contrast,
331 aged *pink1-/-* mice showed no such age-related changes in neuronal ubiquitin distribution or
332 insoluble ubiquitin levels (***Figure 4E, F***). Following MCAO, insoluble ubiquitin levels were
333 significantly elevated in the ipsilateral hemisphere of wildtype mice compared to sham and
334 contralateral hemisphere, but remained unchanged in *pink1-/-* mice (***Figure 4G***).

Protein aggregation is a hallmark of aging and neurodegenerative diseases such as AD (***Hegde et al.*, 2023**); it arises from perturbed proteostasis and can impair proteasomal activity in return. Acute proteasomal inhibition can also result from ischemia or pharmacological treatments. Since sPINK1 is rapidly degraded by functional proteasomes, impaired proteasomes can lead to the accumulation of sPINK1 and pUb, leading to further proteasomal inhibition. Together, our results reveal that *pink1* knockout disrupts this cycle, thereby alleviating proteasomal inhibition and mitigating protein aggregation under these conditions, further demonstrating the critical role of pUb in this process.

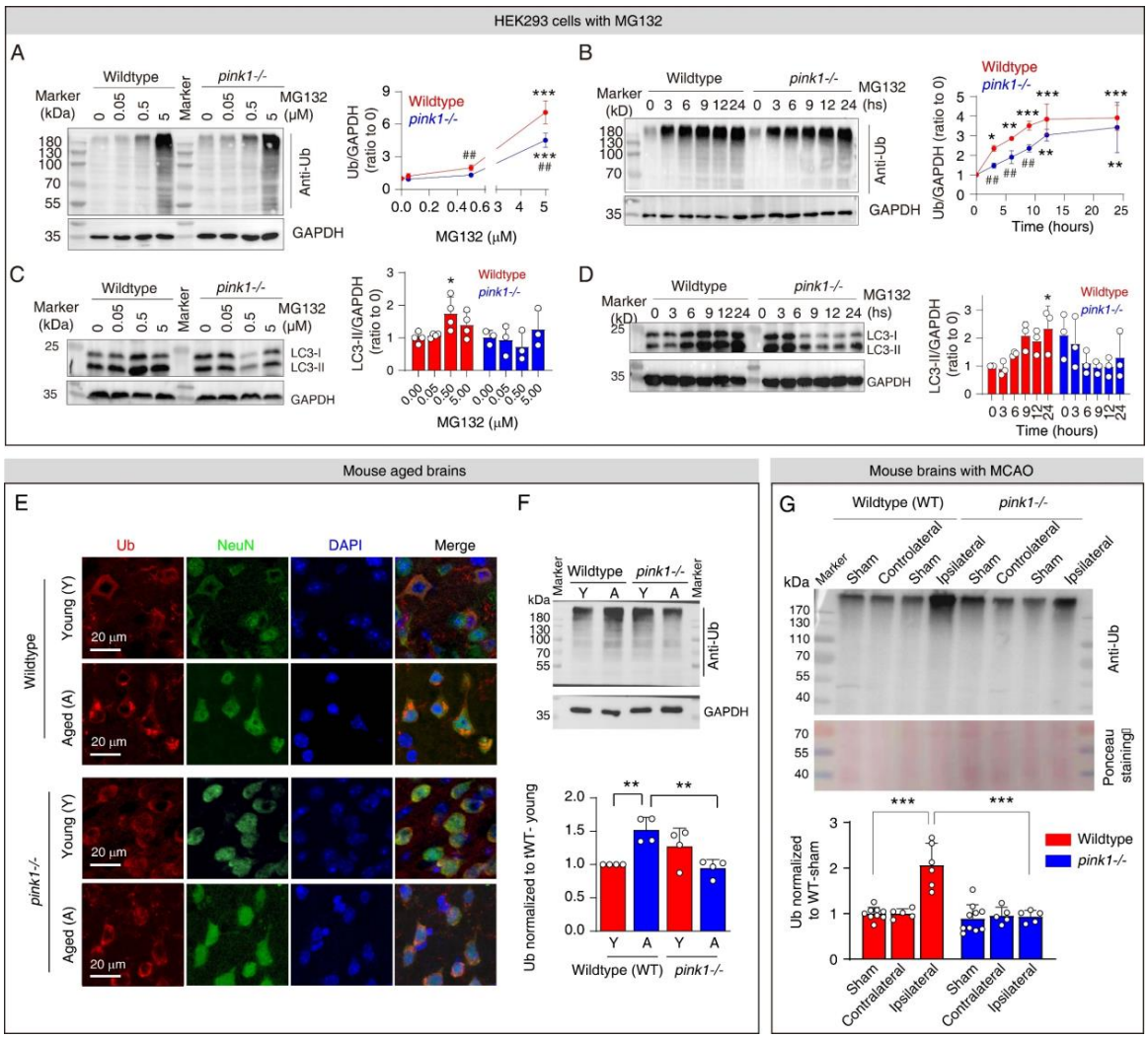


**Figure 4. *pink1* knockout mitigates protein aggregation upon proteasomal inhibition.**

345 **(A)** Western blot analysis of ubiquitin levels in the insoluble protein fraction of HEK293 cells
346 following the treatment with 0-5 μM MG132 for 8 hours. $N$=3; ***$P$<0.001 compared to 0 μM
347 MG132; $^{\#\#}P$<0.01 compared with wildtype cells, one-way ANOVA.

348 **(B)** Western blot analysis of ubiquitin levels in the insoluble protein fraction of HEK293 cells
349 following the treatment with 5 μM MG132 over 24-hour period. $N$=4; *$P$<0.05, **$P$<0.01,
350 ***$P$<0.001 compared to 0 μM MG132; $^{\#\#}P$<0.01 compared with wildtype cells, one-way ANOVA.

351 **(C)** Western blot analysis of LC3 levels in HEK293 cells following the treatment with 0-5 μM
352 MG132 for 8 hours. $N$=4; *$P$<0.05 compared to 0 μM MG132, one-way ANOVA.

353 **(D)** Western blot analysis of LC3 levels in HEK293 cells following the treatment with 5 μM MG132
354 treatment over 24 hours. $N$=3; *$P$<0.05 compared to 0 μM MG132, one-way ANOVA.

355 **(E)** Immunofluorescence staining of ubiquitin taken from layer III-IV in the neocortex of brains from
356 young and aged wildtype and *pink1-/-* mice.

357 **(F)** Western blot analysis quantifying ubiquitin in the insoluble protein fraction of the cortex from
358 young and aged mouse brains. $N$=4; **$P$<0.01, one-way ANOVA.

359 **(G)** Western blot analysis of ubiquitin in the insoluble protein fraction of wildtype and *pink1-/-* mouse
360 brains subjected to MCAO for 2 hours followed by 24 hours of reperfusion. Comparison includes the
361 sham-operated group (same procedure without occlusion). Locations of the analyzed regions
362 (contralateral and ipsilateral) are indicated in ***Figure 1—figure supplementary 1***.

363

364 **sPINK1* over-expression causes cumulative proteome-wide changes**

365 Given the critical role of ubiquitin phosphorylation in proteasomal inhibition and
366 protein aggregation, we sought to confirm these effects using phosphomimetic Ub/S65E
367 mutant in SH-SY5Y cell, a neuroblast-link cell line. Over-expression of sPINK1* or
368 Ub/S65E induced the formation of ubiquitin-positive puncta in cells, similar to the effects of
369 MG132 treatment (***Figure 5—figure supplementary 1***) and the observations in HEK293 cells
370 (***Figure 2G***).

371 To extend our findings, we over-expressed sPINK1*, sPINK1* with Ub/S65A
372 (sPINK1*+Ub/S65A), Ub/S65E, or GFP control in mouse hippocampal neurons using
373 AAV2/9. Specific expression was confirmed through GFP co-localization with NeuN
374 fluorescence in the CA1 region (***Figure 5—figure supplementary 2***). While no visible
375 changes were observed at 10 days post-transfection, significant neuronal loss, based on NeuN

376 immunofluorescence staining, was evident at 30 and 70 days in mice expressing Ub/S65E,
377 but not in other three groups (***Figure 5—figure supplementary 2***). Additionally, Ub/S65E
378 induced glial responses at 30- and 70-days post-transfection, based on GFAP/Iba1
379 immunofluorescence staining and GFAP/CD11b Western blot bands (***Figure 5—figure***
380 ***supplementary 3 and 4***, **respectively**). In contrast, the sPINK1* and sPINK1*+Ub/S65A
381 groups showed an increase in GFAP levels at 70-days post-transfection with no changes in
382 Iba1or CD11b levels, suggesting potential neuronal injury (***Figure 5—figure supplementary***
383 ***3, 4***).

384 To explore the underlying mechanism for neuronal injury, we conducted proteomic
385 analysis of mouse hippocampus at 30- and 70-days post-transfection (***Figure 5—dataset***
386 ***supplementary 1***). Although the total number of proteins identified was similar between the
387 GFP and sPINK1* groups (***Figure 5—figure supplementary 5A-D***), notable differences were
388 observed. For example, the neuronal injury and neuroinflammation marker HMGB1 was
389 elevated at both time points following sPINK1* over-expression, while the mitochondrial
390 marker Tom20 showed a delayed decrease at 70 days, indicative of mitochondrial loss.

391 We also conducted gene set enrichment analysis (GSEA) and found a time-dependent
392 effect of sPINK1* over-expression on mitochondrial function. At 30-days, changes in
393 proteins associated with mitophagy, mitochondrial organization, and respiratory electron
394 transport were observed, suggesting an initial injury and compensatory response to
395 mitochondrial stress (***Figure 5—figure supplementary 5E***). By 70-days, these changes
396 expanded to include broader mitochondrial dysfunction and apoptotic processes, ultimately
397 leading to mitochondrial loss and neuronal injury (***Figure 5—figure supplementary 5E***).

398 Additional gene ontology (GO) analysis revealed extensive proteomic dysregulation
399 upon sPINK1* over-expression (***Figure 5—figure supplementary 5F-H***). At 70-days post-
400 transfection, a large number of proteins were either upregulated or downregulated, indicative
401 of disrupted proteostasis. This can be attributed to proteasomal inhibition or stress response
402 to increased protein aggregates. For example, we observed a significant up-regulation of
403 RNA-binding and RNA-processing proteins. Significantly, many of the up-regulated proteins
404 were associated with impaired synaptic functions and neuronal projections, while down-
405 regulated proteins were linked to myelination, synaptic maturation, and lipid metabolism
406 (***Figure 5—figure supplementary 5F-H***). As these changes were insignificant at 30-days
407 post-transfection (***Figure 5—figure supplementary 5F-H***), the proteomics data indicate a
408 systemic and time-dependent impact upon sPINK1* over-expression on neuronal structure
409 and function, leading to cumulative neuronal injury that mirrors the progressive pathogenesis
410 of neurodegeneration.

411 **Elevated pUb levels promote protein aggregation in mouse hippocampal neurons**

412 To investigate the impact of sPINK1* over-expression on protein homeostasis, we
413 measured the levels of PINK1 and pUb in the mouse hippocampus and evaluated protein
414 aggregation at 30- and 70-days post-transfection. At 30-days following sPINK1* transfection,
415 a distinct band for sPINK1 was observed, accompanied by a significant increase in pUb
416 levels ***(Figure 5A***). At 70-days following sPINK1* transfection, three distinct bands could be
417 observed that likely correspond to sPINK1, full-length PINK1, and ubiquitinated PINK1
418 (***Figure 5B***). The presence of full-length PINK1 indicates mitochondrial injury, and
419 ubiquitinated PINK1 indicates compromised proteasomal activity. The pUb levels were
420 increased by 43.8 % and 59.9 % compared to the control at 30- and 70-days following
421 sPINK1* transfection, respectively. In comparison, the pUb level remained at the control

422 level with the Ub/S65A mutant co-expressed with sPINK1* (***Figure 5C***). Thus, Ub/S65A
423 counteract the proteasomal inhibition induced by sPINK1*, thereby promoting the
424 degradation of sPINK1* and prevent pUb accumulation.

425 Immunofluorescence staining revealed the formation of ubiquitin-positive puncta in
426 hippocampal neurons over-expressing sPINK1*, sPINK1+Ub/S65A, or Ub/S65E (***Figure***
427 ***5D***). The increase of ubiquitin levels in the soluble protein fraction of the hippocampus of
428 brains from the sPINK1*+Ub/S65A group but not in the other groups likely reflects the
429 antibody detection of over-expressed Ub/S65A (***Figure 5E***). On the other hand, the levels of
430 ubiquitin in the insoluble protein fraction were significantly elevated in the sPINK1*,
431 sPINK1*+Ub/S65A, and Ub/S65E groups (***Figure 5F***). Notably, proteins smaller than 70
432 kDa accumulated in the sPINK1* and Ub/S65E groups, indicating an inhibition of ubiquitin
433 chain elongation, consistent with our findings obtained *in vitro* (***Figure 3B***), but not in the
434 sPINK1*+Ub/S65A group. Furthermore, over-expression of Ub/S65E resulted in significant
435 neuronal death and glial proliferation (***Figure 5E and Figure 5-supplementary 2, 3, 4***),
436 despite that the overall pUb levels appear unchanged at 70 days post-transfection (***Figure***
437 ***5D***).

438 It should note that over-expression of sPINK1*, sPINK1*+Ub/S65A, or Ub/S65E had
439 minimal effects on autophagic flux at the animal level, as evidenced by unchanged LC3-II
440 and p62 levels in both soluble and insoluble protein fractions (***Figure 5—figure***
441 ***supplementary 6***). This contrasts with the findings in cultured cells (***Figure 4F, 4G***), and
442 suggests that, mechanistically, protein aggregation driven by elevated pUb levels primarily
443 results from the inhibition of proteasomal degradation in the brains of animal or human with
444 neurodegenerative conditions.

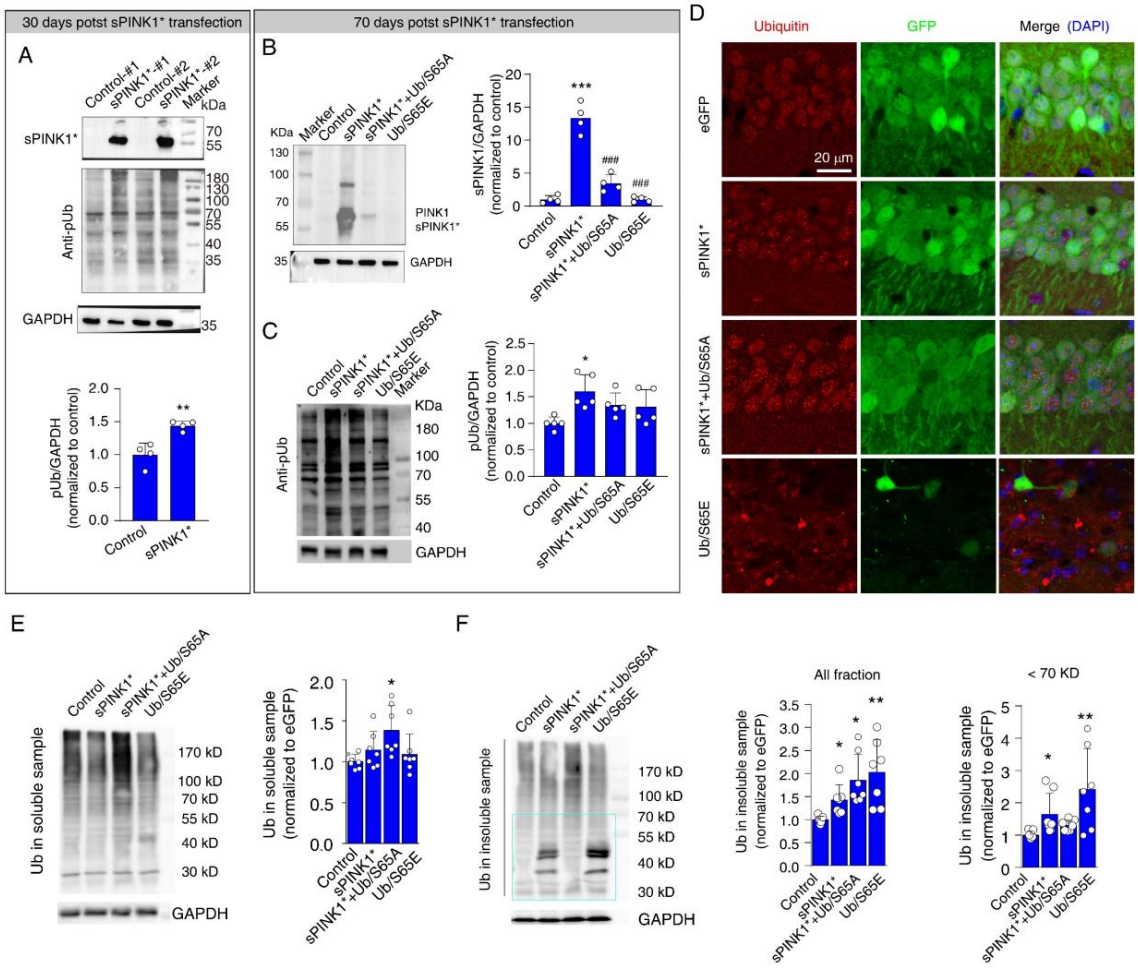


**Figure 5. Elevated pUb levels induce protein aggregation in mouse hippocampal neurons.**

**(A)** Western blot analysis showing the levels of PINK1 and pUb in mouse hippocampus at 30-days post-transfection. *N*=4; ***P*<0.01 compared with control, one-way ANOVA.

**(B)** Western blot analysis of PINK1 in the mouse hippocampus at 70-days post-transfection. *N*=4; ***P*<0.001 compared with control; $^{\#\#\#}P$<0.001 compared with sPINK1, one-way ANOVA.

**(C)** Western blot analysis of pUb in the mouse hippocampus at 70-days post-transfection. *N*=5; **P*<0.05 compared with control, one-way ANOVA.

**(D)** Representative immunofluorescence images depicting ubiquitin staining in the CA1 neurons of the mouse hippocampus at 70-days post-transfection.

**(E)** Western blot analysis of ubiquitin in the soluble protein fraction of hippocampal lysates at 70-days post-transfection. *N*=7; **P*<0.05 compared with control, one-way ANOVA.

**(F)** Western blot analysis of ubiquitin in the insoluble protein fraction of hippocampal lysates at 70-days post-transfection. Quantitative analysis was conducted for total protein at all molecular weight and for proteins with molecular weight <70 kDa. *N*=7; **P*<0.05, ***P*<0.001 compared with control, one-way ANOVA.

462 **Elevated pUb levels impair neuronal integrity and cognitive function**

463 At 70 days post-transfection with sPINK1*, we observed protein aggregation,
464 mitochondrial injury, neuroinflammation and proteome-wide changes (***Figure 5 and Figure***
465 ***5-supplemenatary 2, 3, 4, 5***). To assess the impact of elevated pUb levels on neuronal
466 integrity and cognitive function, we performed behavioral tests on mice at 70-days post-
467 transfection. Over-expression of sPINK1* or Ub/S65E significantly reduced the number of
468 sniffs toward the novel object in novel object recognition test compared to the control mice or
469 the old object (***Figure 6A, B***). In the fear conditioning test, over-expression of sPINK1* or
470 Ub/S65E also significantly reduced freezing time compared to control mice (***Figure 6C, D***).
471 These findings indicate that both sPINK1* and Ub/S65E over-expression impaired cognitive
472 functions of mice. Moreover, co-expression of Ub/S65A with sPINK1* ameliorated
473 sPINK1*-induced cognitive deficits, suggesting a protective effect against pUb-caused
474 impairments (***Figure 6A-D***).

475 Consistent with the proteomics analysis (***Figure 5—figure supplementary 5D***),
476 Western blot analysis showed decreased levels of Tom20, a mitochondrial marker, in brains
477 over-expressing sPINK1* (***Figure 6E***). Notably, the mitochondrial deficit induced by
478 sPINK1* over-expression could be reversed by co-expressing Ub/S65A (***Figure 6E***).
479 Furthermore, we observed reduced levels of MAP2, a dendritic marker, and PSD95, a
480 postsynaptic density marker, in the hippocampus of mice over-expressing sPINK1* and
481 Ub/S65E. The reductions could be restored by co-expressing Ub/S65A with sPINK1*
482 (***Figure 6F, G***). Together, these findings indicate that sPINK1* over-expression induced
483 neuronal injury originating from the nerve terminals, recapitulating neurodegenerative
484 changes. The protective effects conferred upon Ub/S65A co-expression further support the
485 mechanism that the neuronal injury is primarily mediated by elevated pUb levels.

Despite the absence of obvious changes in NeuN immunofluorescence at 70 days post-transfection of sPINK1* (***Figure 5-fingure supplementary 2***), we investigated morphological alternations in nerve terminals using Golgi staining. The staining revealed a reduction in dendritic spine density following sPINK1* over-expression, which was reversed by co-expressing Ub/S65A (***Figure 6H***). In contrast, Ub/S65E over-expression resulted in severe dendritic and spine loss, characterized by marked slimmer dendrites and a significant reduction in spine density (***Figure 6H***). These findings are consistent with the Western blot data showing reduced levels of MAP2 and PSD95 (***Figure 6F, G***).

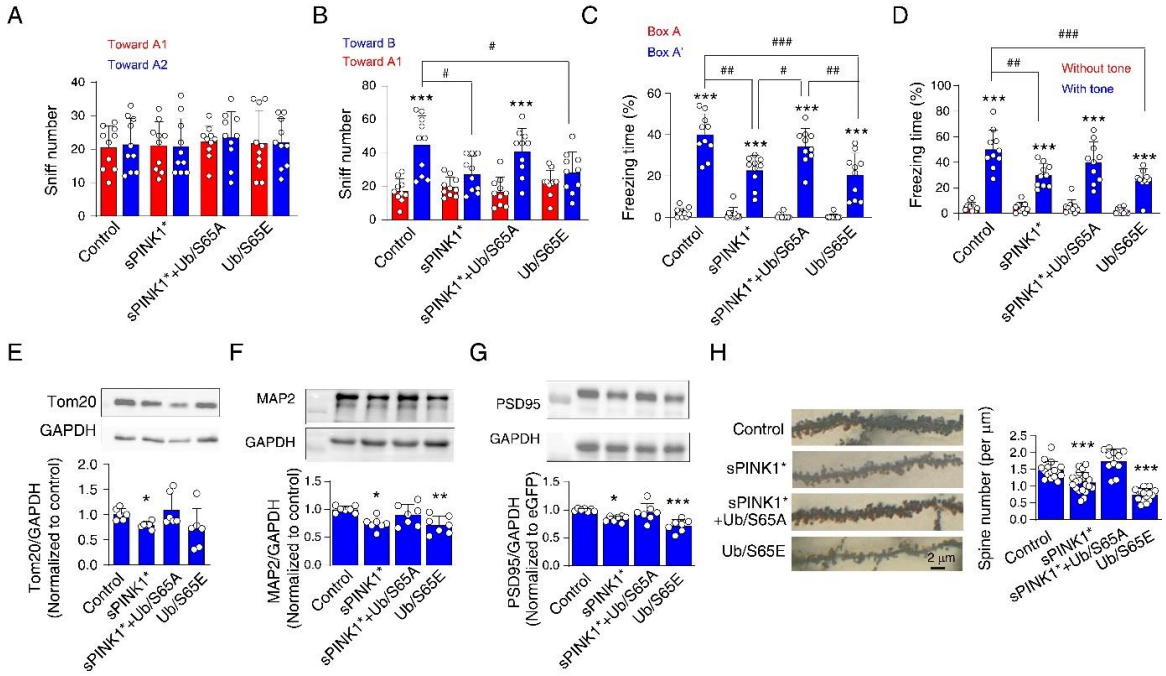


**Figure 6. Elevated pUb levels induce neuronal injury in mouse brains at 70 days post-transfection.**

**(A)** Novel object recognition test showing the number of sniffs toward two distinct objects in the training phase. *N*=10.

**(B)** Novel object recognition test showing the number of sniffs toward the old object (A1) and the novel object (B) in the testing phase. *N*=10; ***$P$<0.001 compared with the sniff number toward A1 object, paired *t*-test. $^{\#}P$<0.05, one-way ANOVA.

**(C, D)** The percentage of freezing time in fear conditioning tests for the evaluation of contextual (C) and cued (D) memory. For contextual memory, the mice were put in the box and received foot shock. For cued memory, the mice were put in a new box, and the same tone accompanying the foot shock was applied. *N*=10; ***$P$<0.001 compared with Box A (contextual) or absence of tone (cued), paired *t*-test. $^{\#}P$<0.05, $^{\#\#}P$<0.01, $^{\#\#\#}P$<0.001, one-way ANOVA.

507 **(E-G)** Western blot analyses to assess levels of mitochondrial, dendritic, and synaptic markers:
508 Tom20 (E), MAP2 (F), and PSD95 (G) in the mouse hippocampus. $N$=7; *$P$<0.05, **$P$<0.01,
509 ***$P$<0.001 compared with control, one-way ANOVA.

510 **(H)** Golgi staining to assess the number of neuronal spines in hippocampal neurons. The left panel
511 shows representative images, and the right panel provides a statistical analysis of spine density on
512 hippocampal neuron dendrites. $N$=11-20 dendrites from 3 mice for each group. ***$P$<0.001 compared
513 with control, one-way ANOVA.

514

515 **sPINK1 over-expression inhibits CamKII-CREB pathway in the hippocampus**

516 The inhibition of proteasomal activity not only impairs protein degradation but also
517 disrupts protein activation by preventing the controlled removal of inhibitory proteins.
518 Notably, our proteomics analysis revealed a >54-fold increase in CamK2n1
519 (Calcium/calmodulin-dependent protein kinase II inhibitor 1, Uniprot Q6QWF9) upon
520 sPINK1* over-expression. CamK2n1 is an endogenous inhibitor of CamKII (***Gouet et al.*,**
521 **2012**), and CamKII is essential for synapse formation, neuronal plasticity, and long-term
522 potentiation (***Hell*, 2014; *O'Day*, 2022**). As illustrated in ***Figure 7A***, the activation of
523 CamKII requires the targeted degradation of CamK2n1 by the proteasome (***Buard et al.*,**
524 **2010**). Then, the increase of phosphorylated CamKII subsequently initiate the CREB signal
525 pathway, representing a key mechanism in synaptic plasticity (***Davidson and Pickering*, 2023;**
526 ***Ortega-Martínez*, 2015**). The over-expression of sPINK1* increases pUb level, which can
527 inhibit CamK2n1 degradation and suppress the activation of CamKII-CREB signal pathway.

528 Immunofluorescence staining confirmed the elevated CamK2n1 levels in hippocampus
529 CA1 neurons at 70 days post-transfection of sPINK1* compared to the controls (***Figure 7B***).
530 This increase was accompanied by reduced levels of phosphorylated CamKII (pCamKII)
531 (***Figure 7C***) and phosphorylated CREB (pCREB) (***Figure 7D***), the latter of which was
532 confirmed by Western blotting (***Figure 7E***). Furthermore, sPINK1* over-expression led to

533 reduced levels of BDNF and ERK, all downstream targets of CREB signaling (***Figure 7F, G***).
534 These findings suggest that impaired degradation of CamK2n1 disrupts CamKII-CREB
535 signaling, contributing to the structural deficits in dendritic spines, postsynaptic density, and
536 neuronal projection.

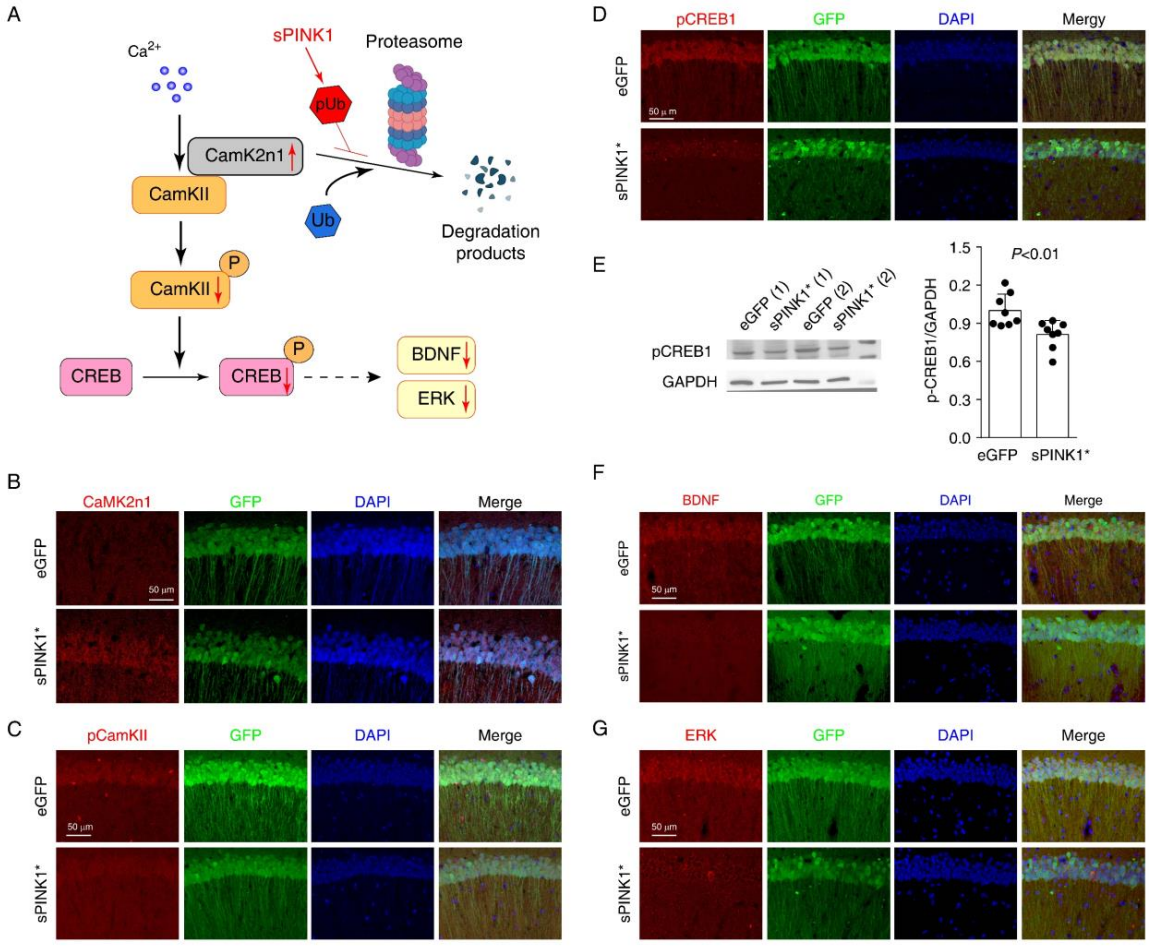

537

538 **Figure 7. Elevated pUb levels inhibit CamKII-CREB signaling in mouse hippocampal neurons.**
539 (A) An illustration of the inhibitory effect on CamK2n1 in the CamKII-CREB1 signaling pathway.
540 (B-D) Immunofluorescence staining of CamK2n1 (B), pCamKII (C), and pCREB1 (D) in the CA1
541 region of hippocampus of mice at 70 days post-transfection. (E) Western blot analysis of pCREB1 in
542 mouse hippocampi. *N*=8, independent *t*-test. (F and G) The immunofluorescence staining of BDNF (F)
543 and ERK (G) in the CA1 region of mouse hippocampus.

544

545

546 ## Discussion

547 In this study, we demonstrate that elevated pUb levels are a common feature in both
548 chronic and acute neurodegenerative conditions. While mitochondrial injury has been
549 established as a mechanism that causes pUb elevation (***Chin et al.*, 2023; *Lambourne et al.*,**
550 **2023**), we have identified an additional pathway—the inhibition of proteasomal degradation
551 leads to the stabilization of sPINK1 in the cytoplasm, where it remains active and
552 phosphorylates ubiquitin.

553 Proteasomal inhibition can arise from many different pathological factors associated
554 with neurodegeneration (***Wilson et al.*, 2023**). For example, cerebral ischemia can cause ATP
555 deficiency, and hypoxia and other secondary effect from oxidative stress can further modify
556 the proteasome and impair its function (***Chen et al.*, 2020; *Wojcik and Di Napoli*, 2004**). In
557 AD, amyloid fibrils can impair proteasomal activities by obstructing the proteasome's
558 substrate entry channel (***McDade et al.*, 2024; *Tseng et al.*, 2008**). Declined proteasomal
559 activity slows the degradation of sPINK1, leading to the elevation of pUb levels in the
560 cytoplasm. Indeed, the elevated pUb levels have been proposed as a biomarker of
561 neurodegeneration (***Fiesel et al.*, 2015; *Hou et al.*, 2018**).

562 Using both *in vitro* and *in vivo* models, we demonstrate that elevated pUb levels, driven
563 by sPINK1* over-expression, inhibit proteasomal activity and exacerbate protein aggregation.
564 Conversely, *pink1* knockout reduced protein aggregation in aged mouse brains, brains
565 subjected to MCAO, and HEK293 cells treated with a proteasome inhibitor. Mechanistically,
566 we show that ubiquitin phosphorylation disrupts two critical processes: (1) the covalent
567 elongation of ubiquitin chains, as previously reported (***Wauer et al.*, 2015b**), and (2) the non-
568 covalent interaction between K48-linked polyUb chains and the proteasome, a novel finding
569 in this study. This dual inhibitory mechanism interferes with the ubiquitination of substrate

570 proteins, the recruitment of ubiquitinated proteins to the proteasome, and ultimately, the
571 proteasomal degradation of substrate proteins. Impaired proteasomal activity further impedes
572 sPINK1 degradation, creating a self-amplifying cycle that drives pUb elevation and
573 progressive proteasomal dysfunction. Although cells have built-in stress responses to
574 perturbation of the ubiquitin-proteasome system (***Hegde et al.*, 1993; *Rai et al.*, 2025**), the
575 disruption caused by elevated pUb levels targets ubiquitin—the central player in the
576 system—and is self-amplifying as proteasomal function deteriorates.

577 Extensive literature has reported that pUb plays a neuroprotective role, wherein PINK1
578 activation in response to mitochondrial damage results in the phosphorylation of ubiquitin
579 and Parkin, initiating mitophagy to remove damaged mitochondria (***Agarwal and Muqit*,**
580 **2022; *Li et al.*, 2023; *Shiba-Fukushima et al.*, 2014**). Accordingly, PINK1 deficiency has
581 been linked to neurodegeneration, prompting the development of small-molecule activators
582 (***Chin et al.*, 2023; *Hertz et al.*, 2024; *Li et al.*, 2023**). However, in the current study, over-
583 expression of sPINK1 resulted in chronic neuronal injury, driven by the reciprocal
584 relationship between proteasomal inhibition and pUb elevation. The progressive decline of
585 proteasomal activity disrupts cellular proteostasis, leading to the accumulation of protein
586 aggregates. In addition to the mechanism of causing mitochondrial damage and inflammation
587 by the protein aggregates, impaired proteasomal activity hinders the degradation of inhibitory
588 proteins and consequently block the activation of key signaling pathways essential for
589 neurogenesis and memory formation. Collectively, our findings reveal that PINK1 can
590 function beyond the established role in mitophagy, and elevated pUb levels are not simply a
591 biomarker of neurodegeneration but a driving force behind progressive neuronal injury and
592 neuroinflammation.

593 The neurotoxic effect upon sPINK1 over-expression is mediated through the ubiquitin
594 phosphorylation. Co-expression of the phospho-null mutant Ub/S65A restored proteasomal
595 activity and even promoted the degradation of the rather stable sPINK1 variant used in the
596 current study. Additionally, Ub/S65A co-expression permitted the formation of longer
597 polyUb chains, further supporting its role in antagonizing ubiquitin phosphorylation. In
598 contrast, over-expression of the phospho-mimetic Ub/S65E mutant caused more severe
599 neuronal damage than sPINK1* over-expression. The difference can be attributed to the 100%
600 increase in pUb mimicry with Ub/S65E, whereas sPINK1*-induced pUb levels are relatively
601 low and subjected to dephosphorylation (***Wall et al.*, 2019; *Wang et al.*, 2018**). Similar toxic
602 effects of Ub/S65E over-expression has been reported in yeast (***Swaney et al.*, 2015**).
603 Moreover, sPINK1* can phosphorylate both free and substrate-conjugated Ub, whereas
604 Ub/S65E only mimics monomeric pUb, further contributing to the heightened detrimental
605 effects of the Ub/S65E mutant.

606 In conclusion, our findings have revealed a novel pathogenetic mechanism of
607 neurodegeneration, driven by a self-amplifying cycle of elevated pUb levels and proteasomal
608 inhibition. This cycle leads to the progressive decline of proteasomal activity and the
609 accumulation of toxic protein aggregates, which may underlie both the sequelae of acute
610 insults and the chronic progression of neurodegenerative diseases. Our results demonstrate
611 that pUb is not merely a consequence of this process but also a critical driver of disease
612 progression. Therefore, targeting the pUb-mediated self-amplifying cycle represents a
613 promising therapeutic strategy to slow or halt the progression of neurodegenerative diseases.

614

615 ## Materials and Methods

616 ### Human brain immunofluorescence staining

617 The human brain cingulate gyrus paraffin section samples include two samples from
618 people with Alzheimer's Disease and two age-matched samples as the control. The samples
619 with AD were obtained from the Netherlands Brain Bank (NBB), Netherlands Institute for
620 Neuroscience, Amsterdam (Project number 1613), and the age matched control samples were
621 obtained from the National Health and Disease Human Brain Tissue Resource Center,
622 Hangzhou, China (Project number CN20240454). All material has been collected from
623 donors for or from whom a written informed consent for a brain autopsy and the use of the
624 material and clinical information for research purposes had been obtained by the NBB and
625 CBB. The detailed information of the donors is provided in Supplementary Table 1. The
626 experiments were conducted with approval from the Ethics Committee of the School of
627 Medicine, Zhejiang University, with the approval number ZJU2023-011.

628 For immunofluorescence staining, the samples was incubated at 62°C overnight to
629 dewax. The samples were then hydrated—Xylene for 3 times, 100% ethanol for 2 times, 95%
630 ethanol for 2 times, 75% ethanol for 2 times, and $ddH_2O$ for 2 times. The samples were
631 placed in EDTA antigen retrieval solution, heated to 95-100°C for 30 minutes, and cooled
632 down at room temperature for 30 minutes. After washing with PBS buffer for 3 times, the
633 samples were placed in 3% $H_2O_2$ solution for 10 minutes. After washing with PBS buffer for
634 3 times, the samples were incubated in 0.3% Triton-X PBS for 30 minutes. After washing
635 with PBS buffer for 3 more times, the samples were permeabilized with 0.3% Tween in PBS
636 for 30 minutes, and rinsed 3 times with PBS to remove the detergent. The samples were
637 incubated in a solution with 5% Sudan black B (Aladdin Biochemical Technology Co., Ltd,
638 S109070-25g, Shanghai, China) and 70% ethanol for 1 min at room temperature.

639 Following PBS rinse, the samples were covered with the blocking solution (5% normal
640 goat serum, 2% bovine serum albumin, 0.1% Tween prepared in TBS-T) for 1 hr. The
641 samples were incubated with rabbit anti-PINK1 antibody (1:200, Novus, Colorado, USA,
642 BC100-494), rabbit anti-pUb antibody (1:200, Millipore, Massachusetts, USA, ABS1513), or
643 mouse anti-Aβ antibody (1:500, Biolegend, California, USA, SIG-39320) at 4 ºC overnight.
644 After washing with PBS for 3 times, the samples were incubated with Cy3-conjugated anti-
645 Rabbit IgG (1:200, Jackson, Pennsylvania, USA, 711-165-152) and fluorescein (FITC)-
646 conjugated anti-mouse IgG (1:200, Jackson, Pennsylvania, USA, 715-096-150) for 2 hours at
647 room temperature. After washing with PBS for 3 times, the samples were mounted on the
648 slides using a ProLong™ Gold Antifade Mountant with DAPI (Invitrogen Corp., Carlsbad,
649 CA, USA). The immunofluorescence images were taken using an Olympus FV100 confocal
650 microscope.

651 **Animals**

652 The C57BL/6J and APP/PS1 mice were purchased from Zhejiang Academy of Medical
653 Science. All mice were kept in the Laboratory Animal Center, Zhejiang University School of
654 Medicine. The mice had free access to water and food in air-conditioned rooms (~26 °C,
655 relative humidity ~50%) on a 12-h light/dark cycle. Mice were handled following the Guide
656 for the Care and Use of the Laboratory Animals of the National Institutes of Health. The
657 experimental protocols were approved by the Ethics Committee of Laboratory Animal Care
658 and Welfare, Zhejiang University School of Medicine, with the approval number
659 ZJU20190138.

660 Using CRISPR-Cas9-mediated genome editing technology (***Cong et al.*, 2013**), the
661 *pink1* gene knockout mice (C57BL/6J) were customized purchased in Transgenic Mouse
662 Laboratory of Laboratory Animal Center of Zhejiang University. Briefly, two sgRNA

663 sequences that target exon 6 of the *pink1* gene were cloned into pX330-U6-Chimeric_BB-
664 CBh-hSpCas9 plasmid (a gift from Feng Zhang (Addgene plasmid # 42230;
665 http://n2t.net/addgene: 42230; RRID: Addgene 42230) using the *Bbsl* restriction site. The
666 sequence of sgRNA1 is 5'-GACAGCCATCTGCAGAGAGG-3', and the sequence of
667 sgRNA2 is 5'-GCAGGCAGGACTCACCTCAG-3'. The knockout of *pink1* gene was
668 confirmed by using DAN genotype, quantitative PCR, and Western blotting.

669 **Mouse hippocampus CA1 injection of Adeno-associated virus (AAV)**

670 The rAAV-EF1a-WPRE-hGH pA (AAV2/9) was used to specifically express proteins
671 within neurons, a bistronic vector expressing GFP and sPINK1* (PINK1/F101M/L102-L581)
672 as two separate proteins. Moreover, the rAAV-EF1a-Ub/S65A-P2A-sPINK1-P2A-EGFP-
673 WPRE-hGH pA can express GFP, sPINK1*, and Ub/S65A as three separate proteins, and
674 rAAV-EF1a-Ub/S65E-P2A-EGFP-WPRE-hGH pA can express GFP and Ub/S65E as two
675 separate proteins.

676 Mice of 9-months old were anesthetized with pentobarbital sodium (80 mg/kg) by
677 intraperitoneal injection (I.p.). Then the mice were fixed on a mouse stereotaxic holder
678 (RWD Life Science Co. LTP, China) for the injection of AAV. The distinct AAV was
679 stereotactically injected bilaterally into the CA1 region using a microinjector (Hamilton
680 syringe) with a 31-gauge needle and micropump (LEGATO 130 syringe pump, KD
681 Scientific). After anesthesia using pentobarbital sodium (100 mg/kg, i.p.), the injections were
682 made at stereotaxic coordinates of Bregma: anterioposterior (AP) = −1.7 mm, mediolateral
683 (ML) =1.5 mm, dorsoventral (DV) = 1.7 mm. A total 0.3 μl AAV ($2.25\times10^{12}$ viral
684 particles/ml) was injected into each side of the hippocampus.

685 **Behavioral tests**

686 Novel object recognition (NOR) was used to evaluate the spatial memory of mice
687 according to the previous report (***Shen et al.*, 2023**). After handling for 5 days, the test was
688 performed on the 68th day post injection. An open-field test system (ViewPoint Behavior
689 Technology, France) was used for NOR detection. During the training, two identical objects
690 (named object A1 and A2, 5 cm' 5 cm' 5 cm blue cone) was placed diagonally. The mouse
691 was placed at the center of the box, and the movement of the mouse was recorded for 10 min.
692 After returning to the home cage for 24 hours, the mouse was put in the same box with one of
693 the objects replaced by a novel object in distinct color and shape (object B, 5 cm' 5 cm' 10 cm
694 yellow cuboid). The sniff number (number of visits) toward the objects was analyzed.
695 The fear conditioning test was performed in the Fear Conditioning System (Coulbourn
696 Instruments, USA) according to the previous report (***Shen et al.*, 2023**). The freezing
697 percentage was recorded during each phase to analyze their memory. During the training
698 phase, the mouse was placed in the box (identified as box A) without any stimulation for 1.5
699 minutes. Then, a tone (3000 Hz, 85 db) was applied for 30 seconds, and an electric shock (1
700 mA) was applied at the final 2 seconds. After the shock, the mouse was kept in box A for 30
701 second, and was put back to the home cage. The testing was performed at 24 hours after
702 training. The mouse was placed back in the box A without any stimulation for 5 minutes,
703 while the freezing percentage in box A indicates contextual memory. Two hours after the test
704 in box A, the mouse was placed in a new box (identified to box B). For the first 2 minutes, no
705 stimulus was given, and subsequently, the same tone (3000 Hz, 85 db) was applied for the
706 following 3 minutes. The freezing percentage in box B without and with tone was used to
707 analyze the cue memory of the mice.

708 **Focal cerebral ischemia/reperfusion**

709 After anesthetized with pentobarbital sodium (80 mg/kg) by intraperitoneal injection
710 (I.p.), the mice were operated with middle cerebral artery occlusion (MCAO) for 2 hours
711 ischemia followed by 24 hours reperfusion. Briefly, a 6-0 nylon monofilament suture was
712 inserted into the internal carotid to occlude the origin of MCA (***Shi et al.*, 2012**). Two hours
713 after occlusion, the suture was withdrawn to allow reperfusion for 24 hours. Mouse body
714 temperature was maintained at 37 °C using a thermostatic pad during and after surgery. In
715 sham-operated mice, the external carotid artery was surgically isolated but the suture was no
716 inserted.

717 **Mouse brain tissue collection**

718 Mice were anesthetized using pentobarbital sodium (150 mg/kg, i.p.). The mouse brains
719 were removed after transcardially perfused with 4 °C saline and freshly prepared 4%
720 paraformaldehyde. The brains were further fixed in 4% paraformaldehyde at 4 °C for one day
721 and transferred to 30% sucrose solution for dehydration. The brains were sliced into 30 μm
722 thick slices by cryomicrotomy (CM1900, Leica, Wetzlar, Germany). The slices were stored
723 at -20°C in the solution (30% glycerol, 30% glycol, 40% PBS) for immunofluorescence and
724 Nissle staining.
725 For Western blotting, the mouse was transcardially perfused only with 4 °C saline. The
726 brains were removed, and the hippocampus was isolated. The hippocampus was quickly
727 frozen in liquid nitrogen and stored at -80 °C until use.

728 **Cell lines, cell culture, and cell transfection**

729 HEK293 cells and SH-SYT5Y cells were purchased from the Institute of Cell Biology
730 of the Chinese Academy of Sciences (Cell Biology of the Chinese Academy of Sciences,

731 Shanghai, China). The *pink1* gene knockout HEK293 cell was homely made using CRISPR-
732 Cas9-mediated genome editing technology(***Ran et al.*, 2013**). PINK1 sgRNA
733 (CCTCATCGAGGAAAAACAGG) was cloned to U6-sgPINK1-mCherry plasmid (a gift
734 from John Doench & David Root (Addgene plasmid # 78038; http://n2t.net/addgene:78038 ;
735 RRID:Addgene_78038). The U6-sgPINK1-mCherry plasmid and PX458-Cas9-EGFP
736 plasmid (a gift from Prof. Feng Zhang (Broad Institute, Cambridge, MA), Addgene plasmid
737 #48138) were co-transfected into HEK293 cells. The mCherry and GFP double-positive cells
738 were single-cell sorted 24 hours post-transfection using an MoFloAstrios EQ cell sorter
739 (Beckman Coulter, US) and grown in separate cultures that were subsequently screened for
740 the presence of frameshift mutations leading to nonsense-mediated decay on both alleles. The
741 *pink1* knockout was confirmed using western blotting.

742 Cells were grown in Dulbecco's modified essential medium (DMEM, Gibco by Thermo
743 Fisher Scientific, C11995500BT) supplemented with 10% heat-inactivated fetal bovine
744 serum (FBS, Zhejiang Tianhang Biotechnology, China, 11011-8611) in the atmosphere of 5%
745 $CO_2$ at 37 °C.

746 Lipo3000 (Invitrogen, California, USA, L3000001) was used to transfect plasmids,
747 following to the manufacturer' protocol. Briefly, an appropriate number of cells were seeded
748 one day before transfection with 70-80% confluent at the time of transfection. Before
749 transfection, plasmid DNA was carefully mixed with 250 μl Opti-MEM (Gibco by Life
750 Technologies, Carlsbad, USA). Subsequently, 250 μl Lipo3000 was carefully mixed with
751 Opti-MEM. The mixture was incubated at room temperature for 25 min. The freshly formed
752 DNA/Lipo3000 precipitates were carefully pipetted to the cells. The medium containing
753 transfection reagents was removed after 6 hours and fresh medium was added.

754 At the end of treatments, the cells on cover slides were washed with 37 °C PBS and then
755 fixed using freshly prepared 4% paraformaldehyde. Subsequently, the cells were stored in
756 PBS under 4 °C for immunofluorescence staining.

757 **Oxygen glucose deprivation and reperfusion (OGD/R)**

758 Cells were washed twice by using glucose-free DMEM (Procell, PM150270) and
759 incubated at 37 °C with the ventilation of 95% $N_2$ and 5% $CO_2$ for 2 hours. The control cells
760 were washed twice by using high glucose DMEM, and incubated in 95% air and 5% $CO_2$
761 under 37 °C for 2 hours. Then the cells were cultured in the high glucose DMEM with 10%
762 FBS in 95% air and 5% $CO_2$ under 37 °C. This was identified as reperfusion.

763 **The construction of Ub-R-GFP plasmid**

764 The Ub-R-GFP is used for the *in vivo* measurement of proteasomal degradation activity, and
765 constructed according to a previous report(***Dantuma et al.*, 2000**). Briefly, the ubiquitin open
766 reading frame was amplified by PCR with the following primers:

767 Sense primer: 5'-GCG GAATTCACCATGCAGATCTTCGTGAAGACT-3'
768 Antisense primer:
769 5'-GCG GGATCCTGTCGACCAAGCTTCCCGCGCCCACCTCTGAGACGGAGTAC-3'
770 The PCR product was cloned into the EcoRI and BamHI sites of the EGFP-N2 vector. Beside
771 the R residue, a 12 amino acid peptide was inserted between ubiquitin and GFP to increase
772 the proteasomal degradation. Thus, the final product is Ub-R-GKLGRQDPPVAT-GFP. The
773 accumulation of GFP protein was determined using Western blot, reflecting proteasomal
774 degradation activity.

775 **Nissl staining**

776 The brain slices were incubated in a mixture of acetone and chloroform (1:1) for 15 min,
777 and then sequentially incubated in 100%, 95%, 70% alcohol for 5 min. The slices were
778 stained for 10 min in Nissl staining containing 0.2% purple crystal (Yuanhang Reagent
779 Factory, Shanghai, China, YHSJ-01- 92) and 0.3% acetic acid. Subsequently, the slices were
780 dehydrated by incubation in 70%, 95%, 100% alcohol. Finally, the slices were put into
781 xylene for 5 min and then mounted with a mixture of neutral resin and xylene (1:1). The
782 images were taken under a microscope (Olympus BX51, Japan).

783 **Immunofluorescence staining**

784 The floating brain slices or cells on the cover glasses were incubated in 0.1% Triton-X
785 PBS for 30 min, and followed by the incubation in 5% donkey serum for 1 hours. The
786 samples were then incubated with mouse anti-ubiquitin antibody (1:200, Santa Cruz
787 Biotechnology, Texas, USA; SC-8017), rabbit anti-pUb antibody (1:200, Millipore,
788 Massachusetts, USA; ABS1513), rabbit anti-PINK1 antibody (1:200, Novus, Colorado, USA;
789 BC100-494), mouse anti-GFAP antibody (1:1000, CST, Pennsylvania, USA; #3670), rabbit
790 anti-Iba1 antibody (1:1000, FUJIFILM Wako Pure Chemical Corporation, Tokyo, Japan;
791 019-19741), rabbit anti-NeuN antibody (1:1000, CST, Pennsylvania, USA; #36662), mouse
792 anti-Aβ (1:500, Biolegend, California, USA, SIG-39320), rabbit anti-pCREB antibody
793 (1:1000, ABclonal Technology, Wuhan, China; AP0019), rabbit anti-ERK1/2 antibody
794 (1:200, ABclonal Technology, Wuhan, China; E-AB-31374), rabbit anti-pCamKII antibody
795 (1:200, ABclonal Technology, Wuhan, China; AP0255), rabbit anti-CamK2n1 (1:200,
796 Thermo fisher, Massachusetts, USA; PA5-23740), and rabbit anti-BDNF antibody (1:200,
797 ABclonal Technology, Wuhan, China; A11028) at 4 °C overnight. After washed with PBS
798 (10 min' 3 times), the samples were incubated with Cy3 AffiniPure Donkey Anti-Mouse IgG
799 (H+L) (1:200, Jackson ImmunoResearch, PA, USA;715-605-150) or Cy3 AffiniPure Goat

800 Anti-Rabbit IgG (H+L) (1:200, Jackson ImmunoResearch, PA, USA;715-605-150; 111-165-
801 003) or Alexa Fluor488 AffiniPure Goat Anti-Rabbit IgG (H+L) (1:200,
802 Jackson ImmunoResearch, PA, USA; 111-545-003) or Alexa Fluor488 AffiniPure Goat Anti-
803 Rabbit IgG (H+L) (1:200, Jackson ImmunoResearch, PA, USA; 715-545-150) for 2 h. After
804 washing with PBS (10 min each for 3 times), the slices were mounted on slides using a
805 ProLong Gold Antifade Mountant with DAPI. The images were taken under an Olympus
806 FV100 confocal microscope (Olympus, Japan) and analyzed using MetaMorph (version
807 7.8.0.0, Molecular Devices, LLC. San Jose, CA 95134 USA).

808 **The preparation of soluble and insoluble protein fractions for Western blot analysis**

809 We prepared the soluble and insoluble protein fractions as described in a previous report
810 (***Wirths*, 2017**). The cells and brain tissues for the Western blot were lysed using RIPA lysis
811 buffer (Beyotime Biotechnology Research Institute, Jiangsu, China; P0013B) with protease
812 inhibitor (Beyotime Biotechnology Research Institute, Jiangsu, China; P1005) and
813 phosphatase inhibitor (Beyotime Biotechnology Research Institute, Jiangsu, China; P1081).
814 The cells were lysed on ice for 30 min, and every 10 min, the cells were gently vortexed. The
815 brain samples were thoroughly homogenized with a precooled TissuePrep instrument (TP-24,
816 Gering Instrument Company, Tianjin, China) for 1 min at 4 °C. Subsequently, the lysate was
817 centrifuged at 12,000 rpm for 30 min at 4 °C. The supernatant was collected as the soluble
818 protein fraction for Western blot analysis.

819 The precipitate was resuspended in 20 μl SDS buffer (2% SDS, 50 mM Tris-HCl, pH7.5)
820 for ultrasonic pyrolysis at 4 °C. The ultrasonic pyrolysis cycle included 10-sec ultrasonic
821 pyrolysis (Diagenode, Seraing, Belgium) and 30-sec interval, for a total of 8 cycles. The
822 samples were then centrifuged at 12,000 rpm for 30 min at 4 °C. The supernatant was
823 collected as the insoluble protein fraction for Western blot analysis.

824 All protein concentration was determined by using BCA Protein Assay Kit according to
825 the instruction (Beyotime Biotechnology, Shanghai, China; P0009).

826 **Western blot analysis**

827 Appropriate protein samples (50-100 μg) were used and separated using SDS-page gel.
828 The separated proteins were transferred to nitrocellulose membrane. The following antibodies
829 were used: mouse anti-ubiquitin antibody (1:800, Santa Cruz Biotechnology, Texas, USA;
830 SC-8017), rabbit anti-pUb antibody (1:1000, Millipore, Massachusetts, USA; ABS1513),
831 rabbit anti-PINK1 antibody (1:1000, Novus, Colorado, USA; BC100-494), mouse anti-GFAP
832 antibody (1:1000, CST, Pennsylvania, USA; #3670), rabbit anti-CD11b antibody (1:1000,
833 Abcam, Cambridge, UK; ab133357), mouse anti-GAPDH antibody (1:5000, Proteintech,
834 Wuhan, China; 60004-1-Ig), mouse anti-MAP2 antibody (1:2000, Millipore, Billerica, MA,
835 USA; AB5622), rabbit anti-PSD95 antibody (1:1000, CST, Pennsylvania, USA; 3450S),
836 rabbit anti-Tom20 antibody (1:1000, Pennsylvania, USA; 42406S), rabbit anti-LC3 antibody
837 (1:1000, Sigma, Massachusetts, USA; L7543), rabbit anti-p62 antibody (1:1000, Abcam,
838 California, USA; ab109012), rabbit anti-pCREB antibody (1:1000, ABclonal Technology,
839 Wuhan, China; AP0019), and mouse anti-FLAG antibody (1:10000, TransGen biotech,
840 Beijing, China; HT201-01). The secondary antibody was HRP-conjugated goat anti-mouse
841 IgG (1:3000, Cell Signaling Technology, MA, USA; 7076S) or HRP-conjugated goat anti-
842 rabbit IgG (1:10000, Jackson ImmunoResearch, PA, USA, 111-035-003).

843 The immunoblots were then detected using ECL reagents (Potent ECL kit,
844 MultiSciences Biotech, Hangzhou, China; P1425) and measured using GBOX (LI-COR,
845 Odyssey-SA-GBOX, NE, USA). The results were normalized to GAPDH or Ponceau
846 staining (Beyotime Biotechnology Research Institute, Jiangsu, China; P0022), or to the
847 eGFP-expression control on the same immunoblot membrane.

848 **Golgi staining**

849 On the 70th-day post-transfection, mice were anesthetized by intraperitoneal injection of
850 pentobarbital sodium (150 mg/kg) before sacrifice. The mouse brain was quickly removed,
851 and the dorsal hippocampus was separated. The hippocampus was immediately fixed in the
852 fixative solution (Servicebio, Wuhan, China, G1101) for over 48 hours.

853 The dorsal hippocampus was sliced with a thickness of 2-3 mm thickness around the
854 injection site. The tissue was gently rinsed with PBS at least 3 times. The hippocampus tissue
855 was then placed in Golgi-cox staining solution (Servicebio, Wuhan, China; G1069), and
856 incubated in a dark for 14 days. The Golgi-cox staining solution was changed 48 hours after
857 the first soak, and every 3 days afterwards. On the14th-day after staining, the tissues were
858 immersed in distilled water for 3 times and then incubated in 80% acetic acid overnight until
859 the tissue became soft. After rinsing with distilled water, the tissue was placed into 30%
860 sucrose.

861 The tissue was cut into 100 μm slices with an oscillating microtome, and the slices were
862 placed on a gelatin slide and dried overnight in the dark. The slices were then treated with
863 ammonia water for 15 min. After washing with distilled water, the slices were incubated in
864 the fixing solution for 15 min. After washing, the slices were sealed using glycerin gelatin.
865 Images were taken using VS120 Virtual Slide Microscope (Olympus, Japan).

866 **The *in vitro* ubiquitin-dependent proteasome degradation**

867 Ubiquitin was prepared as previously described (***Liu et al.*, 2015; *Liu et al.*, 2012**).
868 K48-linked di-ubiquitin and tetra-ubiquitin were prepared following an established protocol
869 (***Pickart and Raasi*, 2005**), with the conjugation reaction catalyzed by 2.5 μM ubiquitin-
870 activating enzyme E1 (Uniprot P22314) and 20 μM ubiquitin-conjugating enzyme E2-25K

871 (Uniprot P61086), in 20 mM pH 8.0 Tris-HCl buffer. Ub/K48R mutant was incorporated as
872 the distant Ub, and Ub/77D mutant was incorporated as the proximal ubiquitin to prepare
873 ubiquitin chain of the desired length. The residue D77 at the C-terminus was removed with
874 hydrolase YUH1. The fusion protein His-TEV-Ub-GFP was prepared recombinantly based
875 on the design previously described (***Dantuma et al.*, 2000; *Inobe et al.*, 2011**). The *Pediculus*
876 *humanus corporis* PINK1 kinase (phPINK1, uniport E0W1I1) was prepared and purified as
877 previously described (***Dong et al.*, 2017; *Wauer et al.*, 2015a**). ubiquitin phosphorylation was
878 confirmed with electrospray mass spectrometry (Agilent G6530 Q-TOF).

879 The 26S proteasome from HEK293 cells was prepared following an established
880 protocol, with the purification tag appended at the C-terminus of Rpn11 (***Guerrero et al.*,**
881 **2006; *Huang et al.*, 2016**). The proteasome activity was assessed with a fluorogenic peptide,
882 N-succinyl-Leu-Leu-Val-Tyr-7-amido-4-methyl coumarin (Sigma, Massachusetts, USA;
883 S6510). A final concentration of 100 nM proteasome and 100 μM proteasome peptide
884 substrate was prepared in the reaction buffer, containing 50 mM Tris-HCl pH 7.5, 4 mM ATP
885 (Sigma- Aldrich, Cat# A6559) and 5 mM $MgCl_2$. The fluorescence intensity of the product
886 was measured by a fluorometer (Horiba Scientific, FluoroMax-4) at an excitation wavelength
887 of 360 nm.

888 For Western blot analysis of GFP, 200 nM proteasomal substrate and 10 nM human
889 26S proteasome were prepared in 20 mM Tris pH 8.0 buffer, with 50 mM NaCl, 5 mM ATP,
890 and 5 mM $MgCl_2$. The mixture was incubated at 37 ° C for 0, 10, 30, 60, 90, and 120 min. At
891 each time point, 20 μL samples were taken for Western blot analysis. A mouse anti-GFP
892 antibody (1:2000, San-Ying Proteintech Group, 66002-1) and an HRP-conjugated goat anti-
893 mouse IgG (1:3000, CST, Pennsylvania, USA; 7076S) were used. ImageJ was used to
894 analyze the band intensities, which are normalized to the initial intensity.

895 The recombinant Ub, pUb (phosphorylated by phPINK1, uniport E0W1I1), Ub/S65A,
896 and Ub/S65E were reacted with 2.5 μM human ubiquitin-activating enzyme E1 and 20 μM
897 ubiquitin-conjugating enzyme 25K in a reaction buffer containing 20 mM Tris-HCl, pH 8.0.
898 The reaction was carried out under standard conditions to promote K48-linked polyubiquitin
899 chain formation. The resulting polyubiquitin chains were analyzed by SDS-PAGE, followed
900 by Coomassie blue staining to visualize the chain formation.

901 **TIRF analysis of ubiquitin-proteasome interaction**

902 The coverslips were prepared following an established protocol (***Roy et al.*, 2008**). Each
903 coverslip was divided into multiple lanes with double-sided tape for parallel detection of the
904 transient association of K48-polyUb-GFP or pK48-polyUb-GFP in the TIRF experiments,
905 thus to ensure repeatability with different proteins added to the same slide. Streptavidin
906 (VWR Life Science, Cat# 97062-808) in imaging buffer at a concentration of 50 μg/ml was
907 loaded; excess unbound streptavidin was washed away. The imaging buffer contains 25 mM
908 Tris-HCl (pH 7.5), 50 mM NaCl, 10 mM MgCl2, 40 mM imidazole, 5 m/mL BSA (Sigma-
909 Aldrich), 2.5 mM ADP (Sigma-Aldrich), and 0.5 mM ATP-γ-S (Sigma-Aldrich), as
910 previously described (***Lu et al.*, 2015**).
911 The purified human 26S proteasome at 20 nM in the imaging buffer was added to the
912 streptavidin-immobilized coverslip, with excess unbound proteins washed away with the
913 imaging buffer. The substrate protein, either K48-polyUb-GFP or pK48-polyUb-GFP, was
914 then added to the coverslip to a final concentration of 400 pM. The imaging was performed
915 on a Nikon A1 TIRF microscope equipped with a 488 nm laser and an EMCCD camera
916 (Andor DU-897). The time series were acquired at 300 ms per frame for a total duration of 2
917 min for each time series. The view area was 512 pixels by 512 pixels (16 by 16 μm), and the
918 experiments were repeated four times on four different proteasome-immobilized cover slides.

919 Only when K48-polyUb-GFP or pK48-polyUb-GFP is associated with the immobilized
920 proteasome, the green puncta can be observed. The puncta density was counted in iSMS
921 software (***Preus et al.*, 2015**) with default settings. The time series of puncta with brightness
922 above a certain threshold (≥ 3000 a.u.) was captured and the dwell time of more than three
923 consecutive frames are selected for counting the overall number of puncta. The dwell times
924 were tabulated in 300 ms bins and fitted with single exponential decay.

925 **Proteomics analysis**

926 Hippocampus samples were rinsed using PBS and lysed in RIPA lysis buffer. The
927 samples were then denatured at 95 °C for 5 min, followed by sonication at 4 °C (3 sec on
928 followed with 3 sec off, with 30% amplitude). The lysate was centrifuged at 16,000 g for 10
929 min at 4 °C, and the supernatant was collected as whole tissue extract. Protein concentration
930 was determined by Bradford protein assay. Extracts from the protein sample (2 g) were
931 trypsin digested.

932 The enriched peptides sample were precipitated in solution A (0.1% formic acid), and
933 was centrifuged at 16,000 g for 10 min. The peptides were separated on a reverse-phase
934 nano-HPLC C18 column (Precolumn, 3 µm, 120 Å, 2x100 i.d.; analysis column, 1.9 µm 120
935 Å, 30 cm x150 µm, i.d.) at a flow rate of 600 nL/min with a 150 min gradient of 7-95%
936 solution B (0.1% formic acid in acetonitrile). For peptide ionization, 2100 V was applied, and
937 a 320 ºC capillary temperature was used. For detection with Q Exactive HF, peptides were
938 analyzed with one full scan (350–1400 m/z, R = 120,000 at 200 m/z) with an automatic gain
939 control target of $3x10^6$ ions, with max injection time of 80 ms, followed by up to 30 data-
940 dependent MS/MS scans with high-energy collision dissociation (target 5 $x10^4$ ions, max
941 injection time 19 ms, isolation window 1.6 m/z, normalized collision energy of 27%),
942 detected in the Orbitrap (R = 15,000 at 200 m/z). Dynamic exclusion time was set as 30 sec.

943 Raw MS data were searched against the mouse National Center for Biotechnology
944 Information (NCBI) Refseq protein database (updated on 2013/07/01, 29764 entries) by the
945 software Thermo Proteome Discoverer 2.1 using Mascot 2.3. The mass tolerances were 20
946 ppm for precursor and 50 mmu for product ions for Q Exactive HF. The search engine set
947 Acetyl(Protein N-term), oxidation(M), Phospho(ST), Phospho(Y) as variable modifications.
948 Trypsin digestion of up to two missed cleavages was allowed. The peptide identifications
949 were accepted at a false discovery rate (FDR) of 1%. Using a label-free approach, a unique
950 peptide was used to represent the absolute abundance of a particular peptide across the
951 sample.

952 For the proteomic data analysis, quantile normalization was applied to eliminate batch
953 effect, and missing values were imputed using the minimum value observed in the dataset.
954 The differentially expressed proteins were defined with the following these criteria: an
955 increase by more than two-fold or decrease by more than 50%. For Gene Set Enrichment
956 Analysis (GSEA) analysis, Gene Ontology (GO) analysis was conducted by GSEApy
957 (version 0.10.5) Python package to evaluate the enriched GO terms. The association of
958 proteins with GO terms was derived from the DAVID database. For Gene Set Enrichment
959 Analysis (GSEA), the ranking metric used was the fold change, and significantly enriched
960 GO terms were filtered with a cutoff *P*-value of 0.05.

961 **Statistical analysis**

962 Data are presented as mean±SD. The number in statistical analysis indicates biological
963 replicates. GraphPad Prism Software (version 6.0, GraphPad Software, San Diego, CA, USA)
964 was used for statistical analysis and plot graphs. The ROUT test was used to identify outliers.
965 The Brown-Forsythe test was used to evaluate the equal variances of the data. D'Agonstino-
966 Pearson omnibus normality test was performed to test the normality of the data. If the data

967 pass the normality test and equal variance test, *t*-test, parametric one-way ANOVA (Tukey
968 multiple comparisons test), or two-way ANOVA (Newman-Keuls multiple comparisons test)
969 was used. If not, nonparametric test (Dunn's multiple comparisons test) was used. Chi-square
970 test was also used to assess the differences in categorical data distributions. $P<0.05$ was
971 considered statistically significant.

## Author contributions

W.P.Z. and C.T. designed the study and wrote the manuscript. C.C., T.Y.G., H.W.Y., Y.Z., T.Y., T.W., and T.F.W. conducted the experiments. Y.B.L. and W.P.Z. analyzed the data at mouse and cellular level. T.T.L. analyzed the proteomic data. C.T. analyzed the data at protein level.

## Acknowledgements

This study was supported by the National Key R&D Program of China (2023YFF1204400) to C.T. and W.P.Z., and (2021YFF1200900) to T.T.L., the National Natural Science Foundation of China (92353304) to C.T. and (32070666) to T.T.L..

## Data availability

All data needed to evaluate the conclusions in the paper are present in the paper and/or the Supplementary Materials.

988 **References**


989 Agarwal S, and Muqit MMK. 2022. PTEN-induced kinase 1 (PINK1) and Parkin: Unlocking
990 a mitochondrial quality control pathway linked to Parkinson's disease. *Curr Opin Neurobiol*
991 **72**: 111-119. https://doi: 10.1016/j.conb.2021.09.005

992 Beilina A, Van Der Brug M, Ahmad R, Kesavapany S, Miller DW, Petsko GA, and Cookson
993 MR. 2005. Mutations in PTEN-induced putative kinase 1 associated with recessive
994 parkinsonism have differential effects on protein stability. *Proc Natl Acad Sci U S A* **102**:
995 5703-5708. https://doi: 10.1073/pnas.0500617102

996 Buard I, Coultrap SJ, Freund RK, Lee YS, Dell'Acqua ML, Silva AJ, and Bayer KU. 2010.
997 CaMKII "autonomy" is required for initiating but not for maintaining neuronal long-term
998 information storage. *J Neurosci* **30**: 8214-8220. https://doi: 10.1523/jneurosci.1469-10.2010

999 Chen C, Qin H, Tan J, Hu Z, and Zeng L. 2020. The Role of Ubiquitin-Proteasome Pathway
1000 and Autophagy-Lysosome Pathway in Cerebral Ischemia. *Oxid Med Cell Longev* **2020**:
1001 5457049. https://doi: 10.1155/2020/5457049

1002 Chin RM, Rakhit R, Ditsworth D, Wang C, Bartholomeus J, Liu S, Mody A, Laishu A,
1003 Eastes A, Tai C, Kim RY, Li J, Hansberry S, Khasnavis S, Rafalski V, Herendeen D, Garda
1004 V, Phung J, de Roulet D, Ordureau A, Harper JW, Johnstone S, Stohr J, and Hertz NT. 2023.
1005 Pharmacological PINK1 activation ameliorates Pathology in Parkinson's Disease models.
1006 *bioRxiv*. https://doi: 10.1101/2023.02.14.528378

1007 Cong L, Ran FA, Cox D, Lin S, Barretto R, Habib N, Hsu PD, Wu X, Jiang W, Marraffini
1008 LA, and Zhang F. 2013. Multiplex genome engineering using CRISPR/Cas systems. *Science*
1009 **339**: 819-823. https://doi: 10.1126/science.1231143

1010 Costa RO, Martins H, Martins LF, Cwetsch AW, Mele M, Pedro JR, Tome D, Jeon NL,
1011 Cancedda L, Jaffrey SR, and Almeida RD. 2019. Synaptogenesis Stimulates a Proteasome-
1012 Mediated Ribosome Reduction in Axons. *Cell reports* **28**: 864-876 e866. https://doi:
1013 10.1016/j.celrep.2019.06.080

1014 Dantuma NP, Lindsten K, Glas R, Jellne M, and Masucci MG. 2000. Short-lived green
1015 fluorescent proteins for quantifying ubiquitin/proteasome-dependent proteolysis in living
1016 cells. *Nat Biotechnol* **18**: 538-543. https://doi: 10.1038/75406

1017 Davidson K, and Pickering AM. 2023. The proteasome: A key modulator of nervous system
1018 function, brain aging, and neurodegenerative disease. *Front Cell Dev Biol* **11**: 1124907.
1019 https://doi: 10.3389/fcell.2023.1124907

1020 Dong X, Gong Z, Lu YB, Liu K, Qin LY, Ran ML, Zhang CL, Liu Z, Zhang WP, and Tang
1021 C. 2017. Ubiquitin S65 phosphorylation engenders a pH-sensitive conformational switch.
1022 *Proc Natl Acad Sci U S A* **114**: 6770-6775. https://doi: 10.1073/pnas.1705718114

1023 Fiesel FC, Ando M, Hudec R, Hill AR, Castanedes-Casey M, Caulfield TR, Moussaud-
1024 Lamodiere EL, Stankowski JN, Bauer PO, Lorenzo-Betancor O, Ferrer I, Arbelo JM, Siuda J,
1025 Chen L, Dawson VL, Dawson TM, Wszolek ZK, Ross OA, Dickson DW, and Springer W.
1026 2015. (Patho-)physiological relevance of PINK1-dependent ubiquitin phosphorylation.
1027 *EMBO Rep* **16**: 1114-1130. https://doi: 10.15252/embr.201540514

1028 Gan ZY, Callegari S, Cobbold SA, Cotton TR, Mlodzianoski MJ, Schubert AF, Geoghegan
1029 ND, Rogers KL, Leis A, Dewson G, Glukhova A, and Komander D. 2022. Activation
1030 mechanism of PINK1. *Nature* **602**: 328-335. https://doi: 10.1038/s41586-021-04340-2

1031 Gao J, Li M, Qin S, Zhang T, Jiang S, Hu Y, Deng Y, Zhang C, You D, Li H, Mu D, Zhang
1032 Z, and Jiang C. 2016. Cytosolic PINK1 promotes the targeting of ubiquitinated proteins to the
1033 aggresome-autophagy pathway during proteasomal stress. *Autophagy* **12**: 632-647. https://doi:
1034 10.1080/15548627.2016.1147667

1035 Gouet C, Aburto B, Vergara C, and Sanhueza M. 2012. On the mechanism of synaptic
1036 depression induced by CaMKIIN, an endogenous inhibitor of CaMKII. *PLoS One* **7**: e49293.
1037 https://doi: 10.1371/journal.pone.0049293

1038 Guerrero C, Tagwerker C, Kaiser P, and Huang L. 2006. An integrated mass spectrometry-
1039 based proteomic approach: quantitative analysis of tandem affinity-purified in vivo cross-
1040 linked protein complexes (QTAX) to decipher the 26 S proteasome-interacting network. *Mol*
1041 *Cell Proteomics* **5**: 366-378. https://doi: 10.1074/mcp.M500303-MCP200

1042 Hegde AN, Duke LM, Timm LE, and Nobles H. 2023. The Proteasome and Ageing. *Subcell*
1043 *Biochem* **102**: 99-112. https://doi: 10.1007/978-3-031-21410-3_5

1044 Hegde AN, Goldberg AL, and Schwartz JH. 1993. Regulatory subunits of cAMP-dependent
1045 protein kinases are degraded after conjugation to ubiquitin: a molecular mechanism
1046 underlying long-term synaptic plasticity. *Proc Natl Acad Sci U S A* **90**: 7436-7440. https://doi:
1047 10.1073/pnas.90.16.7436

1048 Hell JW. 2014. CaMKII: claiming center stage in postsynaptic function and organization.
1049 *Neuron* **81**: 249-265. https://doi: 10.1016/j.neuron.2013.12.024

1050 Herhaus L, and Dikic I. 2015. Expanding the ubiquitin code through post-translational
1051 modification. *EMBO reports* **16**: 1071-1083. https://doi: 10.15252/embr.201540891

1052 Hertz N, Chin R, Rakhit R, Ditsworth D, Wang C, Bartholomeus J, Liu S, Mody A, Laihsu A,
1053 Eastes A, Tai C, Kim R, Li J, Khasnavis S, Rafalski V, Heerendeen D, Garda V, Phung J, de
1054 Roulet D, Ordureau A, Harper JW, Johnstone S, and Stohr J. 2024. Pharmacological PINK1
1055 activation ameliorates Pathology in Parkinson's Disease models. *Res Sq*. https://doi:
1056 10.21203/rs.3.rs-4356493/v1

1057 Hou X, Fiesel FC, Truban D, Castanedes Casey M, Lin WL, Soto AI, Tacik P, Rousseau LG,
1058 Diehl NN, Heckman MG, Lorenzo-Betancor O, Ferrer I, Arbelo JM, Steele JC, Farrer MJ,
1059 Cornejo-Olivas M, Torres L, Mata IF, Graff-Radford NR, Wszolek ZK, Ross OA, Murray
1060 ME, Dickson DW, and Springer W. 2018. Age- and disease-dependent increase of the
1061 mitophagy marker phospho-ubiquitin in normal aging and Lewy body disease. *Autophagy* **14**:
1062 1404-1418. https://doi: 10.1080/15548627.2018.1461294

1063 Huang X, Luan B, Wu J, and Shi Y. 2016. An atomic structure of the human 26S proteasome.
1064 *Nat Struct Mol Biol* **23**: 778-785. https://doi: 10.1038/nsmb.3273

1065 Inobe T, Fishbain S, Prakash S, and Matouschek A. 2011. Defining the geometry of the two-
1066 component proteasome degron. *Nat Chem Biol* **7**: 161-167. https://doi:
1067 10.1038/nchembio.521

1068 Kinger S, Jagtap YA, Kumar P, Choudhary A, Prasad A, Prajapati VK, Kumar A, Mehta G,
1069 and Mishra A. 2024. Proteostasis in neurodegenerative diseases. *Adv Clin Chem* **121**: 270-
1070 333. https://doi: 10.1016/bs.acc.2024.04.002

1071 Komander D, and Rape M. 2012. The ubiquitin code. *Annu Rev Biochem* **81**: 203-229.
1072 https://doi: 10.1146/annurev-biochem-060310-170328

1073 Koyano F, Okatsu K, Kosako H, Tamura Y, Go E, Kimura M, Kimura Y, Tsuchiya H,
1074 Yoshihara H, Hirokawa T, Endo T, Fon EA, Trempe JF, Saeki Y, Tanaka K, and Matsuda N.
1075 2014. Ubiquitin is phosphorylated by PINK1 to activate parkin. *Nature* **510**: 162-166.
1076 https://doi: 10.1038/nature13392

1077 Krishna KK, Behnisch T, and Sajikumar S. 2022. Modulation of the Ubiquitin-Proteasome
1078 System Restores Plasticity in Hippocampal Pyramidal Neurons of the APP/PS1 Alzheimer's
1079 Disease-Like Mice. *J Alzheimers Dis* **86**: 1611-1616. https://doi: 10.3233/JAD-215718

1080 Lambourne OA, Bell S, Wilhelm LP, Yarbrough EB, Holly GG, Russell OM, Alghamdi AM,
1081 Fdel AM, Varricchio C, Lane EL, Ganley IG, Jones AT, Goldberg MS, and Mehellou Y.
1082 2023. PINK1-Dependent Mitophagy Inhibits Elevated Ubiquitin Phosphorylation Caused by

Mitochondrial Damage. *J Med Chem* **66**: 7645-7656. https://doi: 10.1021/acs.jmedchem.3c00555

Lazarou M, Sliter DA, Kane LA, Sarraf SA, Wang C, Burman JL, Sideris DP, Fogel AI, and Youle RJ. 2015. The ubiquitin kinase PINK1 recruits autophagy receptors to induce mitophagy. *Nature* **524**: 309-314. https://doi: 10.1038/nature14893

Li J, Yang D, Li Z, Zhao M, Wang D, Sun Z, Wen P, Dai Y, Gou F, Ji Y, Zhao D, and Yang L. 2023. PINK1/Parkin-mediated mitophagy in neurodegenerative diseases. *Ageing Res Rev* **84**: 101817. https://doi: 10.1016/j.arr.2022.101817

Liu Z, Gong Z, Jiang WX, Yang J, Zhu WK, Guo DC, Zhang WP, Liu ML, and Tang C. 2015. Lys63-linked ubiquitin chain adopts multiple conformational states for specific target recognition. *eLife* **4**: e05767. https://doi: 10.7554/eLife.05767

Liu Z, Zhang WP, Xing Q, Ren X, Liu M, and Tang C. 2012. Noncovalent dimerization of ubiquitin. *Angew Chem Int Ed Engl* **51**: 469-472. https://doi: 10.1002/anie.201106190

Lu Y, Lee BH, King RW, Finley D, and Kirschner MW. 2015. Substrate degradation by the proteasome: a single-molecule kinetic analysis. *Science* **348**: 1250834. https://doi: 10.1126/science.1250834

Mauvezin C, and Neufeld TP. 2015. Bafilomycin A1 disrupts autophagic flux by inhibiting both V-ATPase-dependent acidification and Ca-P60A/SERCA-dependent autophagosome-lysosome fusion. *Autophagy* **11**: 1437-1438. https://doi: 10.1080/15548627.2015.1066957

McDade E, Liu H, Bui Q, Hassenstab J, Gordon B, Benzinger T, Shen Y, Timsina J, Wang L, Sung YJ, Karch C, Renton A, Daniels A, Morris J, Xiong C, Ibanez L, Perrin R, Llibre-Guerra JJ, Day G, Supnet-Bell C, Xu X, Berman S, Chhatwal J, Ikeuchi T, Kasuga K, Niimi Y, Huey E, Schofield P, Brooks W, Ryan N, Jucker M, Laske C, Levin J, Voglein J, Roh JH, Lopera F, Bateman R, and Cruchaga C. 2024. Ubiquitin-Proteasome System in the Different Stages of Dominantly Inherited Alzheimer's Disease. *Res Sq*. https://doi: 10.21203/rs.3.rs-4202125/v1

O'Day DH. 2022. Calmodulin Binding Domains in Critical Risk Proteins Involved in Neurodegeneration. *Curr Issues Mol Biol* **44**: 5802-5814. https://doi: 10.3390/cimb44110394

Okatsu K, Kimura M, Oka T, Tanaka K, and Matsuda N. 2015. Unconventional PINK1 localization to the outer membrane of depolarized mitochondria drives Parkin recruitment. *J Cell Sci* **128**: 964-978. https://doi: 10.1242/jcs.161000

Okatsu K, Uno M, Koyano F, Go E, Kimura M, Oka T, Tanaka K, and Matsuda N. 2013. A dimeric PINK1-containing complex on depolarized mitochondria stimulates Parkin recruitment. *J Biol Chem* **288**: 36372-36384. https://doi: 10.1074/jbc.M113.509653

Ortega-Martínez S. 2015. A new perspective on the role of the CREB family of transcription factors in memory consolidation via adult hippocampal neurogenesis. *Front Mol Neurosci* **8**: 46. https://doi: 10.3389/fnmol.2015.00046

Pickart CM, and Raasi S. 2005. Controlled synthesis of polyubiquitin chains. *Methods Enzymol* **399**: 21-36. https://doi: 10.1016/S0076-6879(05)99002-2

Pohl C, and Dikic I. 2019. Cellular quality control by the ubiquitin-proteasome system and autophagy. *Science* **366**: 818-822. https://doi: 10.1126/science.aax3769

Pollock L, Georgiou LC, Rusilowicz-Jones EV, Clague MJ, and Urbé S. 2024. A long-lived pool of PINK1 imparts a molecular memory of depolarisation-induced activity. *bioRxiv*. https://doi: 10.1101/2024.07.03.601901

Preus S, Noer SL, Hildebrandt LL, Gudnason D, and Birkedal V. 2015. iSMS: single-molecule FRET microscopy software. *Nat Methods* **12**: 593-594. https://doi: 10.1038/nmeth.3435

1130 Rai M, Hunt LC, and Demontis F. 2025. Stress responses induced by perturbation of the
1131 ubiquitin-proteasome system. *Trends Biochem Sci* **50**: 175-178. https://doi:
1132 10.1016/j.tibs.2024.12.011
1133 Ran FA, Hsu PD, Wright J, Agarwala V, Scott DA, and Zhang F. 2013. Genome engineering
1134 using the CRISPR-Cas9 system. *Nat Protoc* **8**: 2281-2308. https://doi:
1135 10.1038/nprot.2013.143
1136 Roy R, Hohng S, and Ha T. 2008. A practical guide to single-molecule FRET. *Nat Methods* **5**:
1137 507-516. https://doi: 10.1038/nmeth.1208
1138 Samant RS, Livingston CM, Sontag EM, and Frydman J. 2018. Distinct proteostasis circuits
1139 cooperate in nuclear and cytoplasmic protein quality control. *Nature* **563**: 407-411. https://doi:
1140 10.1038/s41586-018-0678-x
1141 Shen C, Chen C, Wang T, Gao TY, Zeng M, Lu YB, and Zhang WP. 2023. The Depletion of
1142 NAMPT Disturbs Mitochondrial Homeostasis and Causes Neuronal Degeneration in Mouse
1143 Hippocampus. *Mol Neurobiol* **60**: 1267-1280. https://doi: 10.1007/s12035-022-03142-5
1144 Shi WZ, Qi LL, Fang SH, Lu YB, Zhang WP, and Wei EQ. 2012. Aggravated chronic brain
1145 injury after focal cerebral ischemia in aquaporin-4-deficient mice. *Neurosci Lett* **520**: 121-
1146 125. https://doi: 10.1016/j.neulet.2012.05.052
1147 Shiba-Fukushima K, Arano T, Matsumoto G, Inoshita T, Yoshida S, Ishihama Y, Ryu KY,
1148 Nukina N, Hattori N, and Imai Y. 2014. Phosphorylation of mitochondrial polyubiquitin by
1149 PINK1 promotes Parkin mitochondrial tethering. *PLoS Genet* **10**: e1004861. https://doi:
1150 10.1371/journal.pgen.1004861
1151 Shiba-Fukushima K, Ishikawa KI, Inoshita T, Izawa N, Takanashi M, Sato S, Onodera O,
1152 Akamatsu W, Okano H, Imai Y, and Hattori N. 2017. Evidence that phosphorylated ubiquitin
1153 signaling is involved in the etiology of Parkinson's disease. *Hum Mol Genet* **26**: 3172-3185.
1154 https://doi: 10.1093/hmg/ddx201
1155 Soykan T, Haucke V, and Kuijpers M. 2021. Mechanism of synaptic protein turnover and its
1156 regulation by neuronal activity. *Curr Opin Neurobiol* **69**: 76-83. https://doi:
1157 10.1016/j.conb.2021.02.006
1158 Swaney DL, Rodriguez-Mias RA, and Villen J. 2015. Phosphorylation of ubiquitin at Ser65
1159 affects its polymerization, targets, and proteome-wide turnover. *EMBO Rep* **16**: 1131-1144.
1160 https://doi: 10.15252/embr.201540298
1161 Swatek KN, and Komander D. 2016. Ubiquitin modifications. *Cell Res* **26**: 399-422.
1162 https://doi: 10.1038/cr.2016.39
1163 Takatori S, Ito G, and Iwatsubo T. 2008. Cytoplasmic localization and proteasomal
1164 degradation of N-terminally cleaved form of PINK1. *Neurosci Lett* **430**: 13-17. https://doi:
1165 10.1016/j.neulet.2007.10.019
1166 Tang C, and Zhang WP. 2020. How Phosphorylation by PINK1 Remodels the Ubiquitin
1167 System: A Perspective from Structure and Dynamics. *Biochemistry* **59**: 26-33. https://doi:
1168 10.1021/acs.biochem.9b00715
1169 Tseng BP, Green KN, Chan JL, Blurton-Jones M, and LaFerla FM. 2008. Abeta inhibits the
1170 proteasome and enhances amyloid and tau accumulation. *Neurobiol Aging* **29**: 1607-1618.
1171 https://doi: 10.1016/j.neurobiolaging.2007.04.014
1172 Wall CE, Rose CM, Adrian M, Zeng YJ, Kirkpatrick DS, and Bingol B. 2019. PPEF2
1173 Opposes PINK1-Mediated Mitochondrial Quality Control by Dephosphorylating Ubiquitin.
1174 *Cell Rep* **29**: 3280-3292 e3287. https://doi: 10.1016/j.celrep.2019.10.130
1175 Wang L, Cho YL, Tang Y, Wang J, Park JE, Wu Y, Wang C, Tong Y, Chawla R, Zhang J,
1176 Shi Y, Deng S, Lu G, Wu Y, Tan HW, Pawijit P, Lim GG, Chan HY, Zhang J, Fang L, Yu H,

1177 Liou YC, Karthik M, Bay BH, Lim KL, Sze SK, Yap CT, and Shen HM. 2018. PTEN-L is a
1178 novel protein phosphatase for ubiquitin dephosphorylation to inhibit PINK1-Parkin-mediated
1179 mitophagy. *Cell Res* **28**: 787-802. https://doi: 10.1038/s41422-018-0056-0

1180 Wauer T, Simicek M, Schubert A, and Komander D. 2015a. Mechanism of phospho-
1181 ubiquitin-induced PARKIN activation. *Nature* **524**: 370-374. https://doi:
1182 10.1038/nature14879

1183 Wauer T, Swatek KN, Wagstaff JL, Gladkova C, Pruneda JN, Michel MA, Gersch M,
1184 Johnson CM, Freund SM, and Komander D. 2015b. Ubiquitin Ser65 phosphorylation affects
1185 ubiquitin structure, chain assembly and hydrolysis. *EMBO J* **34**: 307-325. https://doi:
1186 10.15252/embj.201489847

1187 Wilson DM, 3rd, Cookson MR, Van Den Bosch L, Zetterberg H, Holtzman DM, and
1188 Dewachter I. 2023. Hallmarks of neurodegenerative diseases. *Cell* **186**: 693-714. https://doi:
1189 10.1016/j.cell.2022.12.032

1190 Wirths O. 2017. Extraction of Soluble and Insoluble Protein Fractions from Mouse Brains
1191 and Spinal Cords. *Bio Protoc* **7**: e2422. https://doi: 10.21769/BioProtoc.2422

1192 Wojcik C, and Di Napoli M. 2004. Ubiquitin-proteasome system and proteasome inhibition:
1193 new strategies in stroke therapy. *Stroke* **35**: 1506-1518. https://doi:
1194 10.1161/01.STR.0000126891.93919.4e

1195 Yamano K, and Youle RJ. 2013. PINK1 is degraded through the N-end rule pathway.
1196 *Autophagy* **9**: 1758-1769. https://doi: 10.4161/auto.24633

1197